

## Article

# “Military Parade Blue Skies” in Beijing: Decisive Influence of Meteorological Factors on Transport Channel and Atmospheric Pollutant Concentration Level

Shujian Yang <sup>1,2</sup> , Yang Zhang <sup>1,2,3,\*</sup>, Jing Shang <sup>4</sup>, Zhengqiang Li <sup>5</sup> , Benjamin de Foy <sup>6</sup>, James Jay Schauer <sup>7</sup> and Yuanxun Zhang <sup>1,2,3,\*</sup>

- <sup>1</sup> College of Resources and Environment, University of Chinese Academy of Sciences, Beijing 100049, China; yangshujian14@mails.ucas.ac.cn
- <sup>2</sup> Yanshan Earth Critical Zone and Surface Fluxes Research Station, Chinese Academy of Sciences, Beijing 101400, China
- <sup>3</sup> National Engineering Laboratory for VOCs Pollution Control Material & Technology, Beijing 101400, China
- <sup>4</sup> Institute of Urban Meteorology, China Meteorological Administration, Beijing 100081, China; jshang@ium.cn
- <sup>5</sup> Institute of Remote Sensing and Digital Earth, Chinese Academy of Sciences, Beijing 100094, China; lizq@radi.ac.cn
- <sup>6</sup> Department of Earth and Atmospheric Sciences, Saint Louis University, Saint Louis, MO 63108, USA; benjamin.defoy@slu.edu
- <sup>7</sup> Wisconsin State Laboratory of Hygiene, University of Wisconsin-Madison, Madison, WI 53706, USA; jjschauer@wisc.edu
- \* Correspondence: zhangyang@ucas.ac.cn (Y.Z.); yxzhang@ucas.ac.cn (Y.Z.); Tel.: +86-10-6967-2963 (Y.Z.); +86-10-8825-6365 (Y.Z.)



**Citation:** Yang, S.; Zhang, Y.; Shang, J.; Li, Z.; de Foy, B.; Schauer, J.J.; Zhang, Y. “Military Parade Blue Skies” in Beijing: Decisive Influence of Meteorological Factors on Transport Channel and Atmospheric Pollutant Concentration Level. *Atmosphere* **2021**, *12*, 636. <https://doi.org/10.3390/atmos12050636>

Academic Editors: Begoña Artíñano, Mizuo Kajino, Ashok Luhar and Makiko Nakata

Received: 28 February 2021  
Accepted: 12 May 2021  
Published: 17 May 2021

**Publisher’s Note:** MDPI stays neutral with regard to jurisdictional claims in published maps and institutional affiliations.



**Copyright:** © 2021 by the authors. Licensee MDPI, Basel, Switzerland. This article is an open access article distributed under the terms and conditions of the Creative Commons Attribution (CC BY) license (<https://creativecommons.org/licenses/by/4.0/>).

**Abstract:** The severity of high atmospheric pollution has been a major social problem in northern China. To improve the air quality in the Beijing–Tianjin–Hebei (BTH) region and guarantee a suitable environment during the military parade and other celebrating activities for the 70th anniversary of the victory for anti-Fascist Warcraft in the year 2015, a series of strict air quality control policies were carried out. To analyze the reduction extents of PM<sub>2.5</sub> and organic matter components during the control period and to examine the meteorological conditions in this region and their decisive influence on the air quality, PM<sub>2.5</sub> samples were collected and the Lagrangian particle dispersion model FLEXPART was performed to calculate potential source locations within the BTH region. PM<sub>2.5</sub>, organic carbon (OC), elementary carbon (EC), and three species types were specifically analyzed. Although the results showed that PM<sub>2.5</sub>, OC, and EC reduced by 64.55%, 48.74%, and 60.75% during the control period, the air mass transport patterns showed great difference at certain periods, which altered the dominant transport direction of air mass and the potential source region of pollutants and organic matters. This alteration completely changed major atmospheric pollutants sources contribution and caused huge concentration changes. Parallel cases also showed that meteorological conditions could avoid massive atmospheric transported from a major emission source region to a receptor site. The meteorological conditions changed the main contribution source region in control and non-control periods and proved the air quality control measures were less necessary in some southern Hebei cities during special events periods.

**Keywords:** PM<sub>2.5</sub>; organic matter; control policies; air quality; Lagrangian particle dispersion model; transboundary transport

## 1. Introduction

Environmental problems have gained people’s attention with the rapid pace of economic development and industrial systems. Air pollutants emitted from industrial systems and human activities generate particulate matter, which are the most important air pollutant resources. The occurrence of frequent haze events has been a most focused air pollution problem, especially in northern China. This region has the most typical high incidence area

of heavy pollution events in East Asia and is also one of the regions with relatively high emission intensity. Additionally, for the spatial and temporal distribution characteristics of the concentration of air pollutants in typically heavily polluted areas, some researchers have carried out detailed and thorough studies based on multiple technical methods. Li et al. [1] analyzed aerosol-related emission characteristics for six cities in both North America and East Asia using satellite and ground data, and future trend predictions were made using models, while potential driving forces of aerosol loading were investigated. Some scholars have also compared the contribution of air pollutant emissions from three major industrial zones in mainland China to the transmission of PM<sub>2.5</sub> in Taiwan based on the air quality model [2]. The pollution characteristics of dust weather in Tianjin and its surrounding areas in northern China and the related potential source areas have also become the topics of some researchers [3]. At the same time, some advanced and special technologies, such as satellite images, were applied to analyze the spatial distribution of PM<sub>2.5</sub> in densely populated areas and heavy traffic areas in specific regions of North America [4]. In the hope of protecting international activities and control air pollution, the Beijing Municipal administration applied severe air quality control policies during such events, such as the Beijing Olympic Games 2008, the APEC summit 2014, and the World Field Championship 2015. Some researchers looked into the air quality in Beijing during each special control period and performed massive assessment research on the reduction effects. Analysis was performed [5] on air quality and meteorological conditions during the Beijing Field Championship 2015 and the Military Parade in Beijing city. The influence of the emission reduction measures on NO<sub>x</sub> concentration was assessed. Several air pollutants and mass concentrations were analyzed [6] during the Military Parade and the improvements of PM<sub>2.5</sub> concentration level were assessed. Simulations were also applied [7] on PM<sub>2.5</sub> properties in Beijing city and the researchers estimated the effects of pollution control measures. The chemical reactions producing PM<sub>2.5</sub> should be largely influenced by the reduction of pollutants emission. Whereas some researchers focused on the Beijing area, some others conducted case studies on air quality improvements from the surrounding area under control policies. Some researchers [8] investigated features of soluble ions in Tianjin during APEC. Some researchers focused on source apportionment on atmospheric fine particles in Shijiazhuang during the Military Parade 2015 [9]. Handan, Hebei was also set as an example [10] for environmental meteorological condition analysis during the Military Parade 2015. Effects of emergency control measures were assessed. Additionally, Lv et al. [11] conducted source apportionment and feature study on PM<sub>2.5</sub> during the Military Parade period in Tangshan. Some researchers investigated visibility level variation during the Beijing APEC period and did reduction assessments [12]. Most of these studies proved that during the air quality control period, PM<sub>2.5</sub> and components concentration levels reduced significantly. However, meteorological conditions were also proven as another major factor influencing the air quality in the BTH area under certain air quality control policies. The meteorological conditions would finally form air mass transport patterns in which atmospheric pollutants could accumulate amongst such transport channels. Some researchers also conducted studies on this topic. Some studies [13] used vertical observation methods to analyze the vertical transport pattern among the APEC periods. The ground-level observation of meteorological conditions and air quality could not fully explain the pollution process, while vertical parameters improved the understanding of regional transport influence on heavy pollution processes. Model simulations and ground-based observation data were both used to quantify the reduction contribution of meteorological conditions under control policies [14]. HYSPLIT and other trajectory models were also applied to examine the contribution of regional transport patterns. Such efforts could partially explain the quantitative contributions of meteorological and control policy [15]. However, thorough studies and methods are still required to assess the actual quantitative reduction contribution of temporary air quality control policies given the regional transboundary transport patterns.

The year 2015 is the 70th anniversary for the victory of the anti-Fascist War. A series of celebration activities were held in Beijing in honor of this historical event, including the Military Parade on Tiananmen square on the date of 3 September. During this period (20 August–4 September), BTH governments applied temporary air quality control measures. Common control measures were applied from 20 August–4 September and more rigorous control measures were added during the military parade event from 1–4 September. During this period, 80% of government vehicles were banned from the roads throughout the day. Private vehicles were half banned according to the odd-and-even-license-plate-rule. The industrial factories and construction fields also ceased working in this period. Moreover, the traffic administration of civil aviation conducted forbidding or detouring measures on the Capital National Airport and the Nanyuan Airport.

We set up offline sampling site and collected PM<sub>2.5</sub> off-line samples during this period to analyze the PM<sub>2.5</sub> and organic matter concentration variation and assess the control effects. A Lagrangian particle model was applied to calculate the transboundary transport patterns and assess the impacts of certain transport paths during the whole sampling period. Parallel simulation cases were performed to calculate historical air-mass transport patterns and identify the meteorological conditions influences.

## 2. Material and Methods

### 2.1. Experiments

Our off-line sampling site was located at the Institute of Remote Sensing and Digital Earth (RADI) of the Chinese Academy of Sciences in the Olympic Village campus of the University of Chinese Academy of Sciences (UCAS). Two samplers were set up to obtain filter samples to collect PM<sub>2.5</sub> and organic matter concentration. The whole sampling period was from 20:00 12 August to 20:00 19 September. Online monitoring data were also collected from the monitoring systems located at the RADI next to our sampler instruments. The online data were gathered hourly and were averaged in parallel with our sampling frequency as a calibration.

PM<sub>2.5</sub> concentrations were calculated using a medium-volume off-line sampler which used 47mm filters and the volume was 21 L/min. All filters were weighed by a 1/100,000 g balance before and after the campaign to calculate the mass value. Quality control and assessment were performed to guarantee the concentration data precision.

A high-volume sampling instrument was set up to collect 150 mm quartz filters for organic matter detection. These quartz filters were used for OC and elementary EC detection and organic matter species analysis. Round 37 mm diameter slices were punched from each 150 mm filter for organic species analysis. A standard pre-processing method was applied for extracting organic matter. The whole extraction process can be divided into five steps, supersonic extraction, concentration, filtration, nitrogen evaporation, and derivation for polar organic species. Detailed descriptions have been discussed in several previous papers [16–21]. GC-MS (Thermo Fisher Scientific, US) instrument was applied for organic matter species detection. The detection column is a TG-1MS GC column with a 30 m × 0.25 mm dimension. The single detection duration time is 80 min for each sample. Further investigations into detection methods have also been discussed in previous papers [16–18,20–22]. A semi-continuous carbon analyzer (model RT-3254, Sunset Laboratory) was used for OC and EC detection. The concentration units can be converted to µg/m<sup>3</sup> by the ratio between the punch area and the filter area. Detailed descriptions of the OC and EC detection by this method have been presented in previous papers [23–25].

To further analyze the primary and secondary organic matter sources and their corresponding concentration trends. We applied the organic matter tracer method [26,27] to calculate the contributions of primary and secondary OC. The calculation equation is as below:

$$[\text{OC}]_{\text{sec}} = [\text{OC}]_{\text{tot}} - [\text{EC}] \times [\text{OC}/\text{EC}]_{\text{pri}} \quad (1)$$

$$[\text{OC}]_{\text{pri}} = [\text{EC}] \times [\text{OC}/\text{EC}]_{\text{pri}} \quad (2)$$

$[\text{OC}]_{\text{sec}}$  is the estimated concentration of secondary organic carbon (SOC).  $[\text{OC}]_{\text{tot}}$  is the OC concentration.  $[\text{EC}]$  stands for EC concentration.  $[\text{OC}/\text{EC}]_{\text{pri}}$  is the estimated concentration of primary organic carbon (POC).  $[\text{OC}/\text{EC}]_{\text{pri}}$  is the OC/EC value from primary sources. We applied the lowest level of OC/EC value for the calculation.

## 2.2. Model Simulation

The Lagrangian particle model FLEXPART (version 3.3.2) [28] was applied to calculate the air mass,  $\text{PM}_{2.5}$ , gaseous compounds, OC, and EC transport features during the whole sampling period to further identify the long-range transboundary transport paths and the potential source region contributions. WRF model (version 3.6.1) [29] provided meteorological fields for the FLEXPART model. We used the new Thompson scheme for microphysics process, the new RRTMG scheme for long and short-wave physics, the YSU scheme for planet boundary layer physics, Noah Land Surface Model for surface physics, Xu–Randall method for the cloud fraction, and the Grell 3D scheme for cumulus clouds. A 2-domain nested simulation was performed. The mother domain had a 27 km resolution and  $90 \times 80$  grids settings covering most of northeast Asia. The inner domain has a 9 km resolution with  $106 \times 91$  grids covering the BTH region. FLEXPART simulations were performed precisely to match the sampling frequency. The particle release period was 1 h and the diffusion period was 48 h. MATLAB was applied to do post-processing work for the output files of FLEXPART. We adopted a novel post-processing method [30–32] to calculate the potential transport channel and corresponding contribution source region. The basic operating principle of the method is to release a certain number of particles within a specific receptor point, and the particle is free to diffuse backward in the atmosphere for a certain amount of time. After reaching the diffusion time, the model outputs the longitude and latitude coordinates of all particles in each timeframe, which is actually the backward trajectory cluster before the air mass is transmitted to the receptor point. Using MATLAB matrix calculation function, the longitude and latitude coordinates of the particles can be converted into an estimate of the amount of time that all particles stay in a particular matrix grid, proportional to the length of time that the air mass stays in each grid before reaching the receptor point. It is called residence time analysis RTA.  $\text{PM}_{2.5}$ , gaseous compounds, OC, and EC transport patterns can then be further calculated by a concentration analysis (CFA) fields algorithm that can highlight the potential atmospheric pollutants source regions. Pollutants' transport paths and corresponding contribution percentages can be calculated via these RTA and CFA matrix fields. Detailed method descriptions and cases with the algorithms have been discussed in several previous papers [28,30–36].

To further demonstrate the impacts of meteorological conditions changes, the FLEXPART method was applied in parallel at the year 2014 and 2016 with the same period (12 August–20 September), whereas we used online monitoring  $\text{PM}_{2.5}$  data for CFA instead of offline sampling data. The online  $\text{PM}_{2.5}$  data were from the Olympic Park monitoring site of the Beijing Municipal Ecological and Environmental Monitoring system. The monitoring site was also the particle release site and only 3 km distance away from the sampling site, which can be considered located in the same meteorology system. Both parallel cases were applied with the same model configurations and set-ups. RTAs and CFAs with  $\text{PM}_{2.5}$  were also calculated using the same algorithms as in 2015. The  $\text{PM}_{2.5}$  concentration were also averaged following the three periods to investigate the emission level at the same time in three years.

## 3. Results and Discussion

For the convenience of the results analysis work, the whole sampling period was divided into three periods according to the air quality control policies: before (13–19 August), during (20 August–4 September), and after (5–19 September) the control period. Concentration data were also analyzed in accordance with three periods.

### 3.1. PM<sub>2.5</sub>, OC, EC and Gaseous Compounds

The concentration time series of the online and offline PM<sub>2.5</sub> data (Figure 1a) showed great agreement with each other. Which confirmed our QA and QC process effective during the sampling and weighing process. The PM<sub>2.5</sub>, OC, and EC concentration data all showed the same trends in the whole sampling period with a significant reduction rate during the control period and increased after the control period (Figure 1b). Two time periods of 12–13 August and 16–17 September both reached the highest concentration for PM<sub>2.5</sub> and that is the same trend with OC and EC, though OC and EC have longer concentration peak in these two time periods. The correlation (Figure 2a,b) showed PM<sub>2.5</sub> have significant relations with OC and EC, with the R<sup>2</sup> value of 0.8543 and 0.8176. The RMSE and MAE values between PM<sub>2.5</sub> and the two also showed that the correlation between the two components and PM<sub>2.5</sub> was within a very reliable range. OC and EC also showed a high correlation of R<sup>2</sup> value 0.8787. The RMSE and MAE values between them were also within a reasonable and credible range, which helped to indicate the reliability of our data. This convincingly implied that the intensity of the organic and PM<sub>2.5</sub> sources are sharing averagely the same potential source region and the source intensity. The emission level variation should affect directly and equally the pollutants concentration level. However, the precise source region and emission intensity would still differ in certain areas and periods considering some quantitative variation difference of PM<sub>2.5</sub> and organic matter.

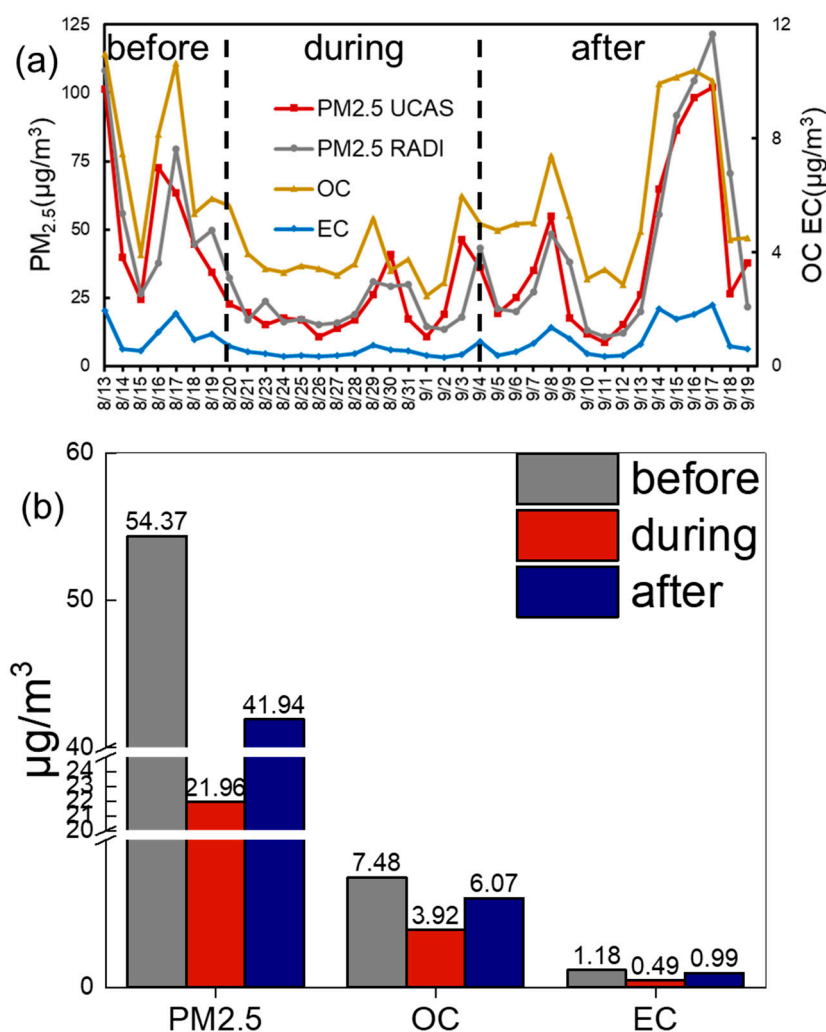


**Figure 1.** (a) shows the concentration of PM<sub>2.5</sub>, OC, and EC concentration from off-line samples and online monitoring system from RADi. The dashed lines are the time boundaries of three periods. (b) shows the average concentration of PM<sub>2.5</sub>, OC, and EC in 3 periods.

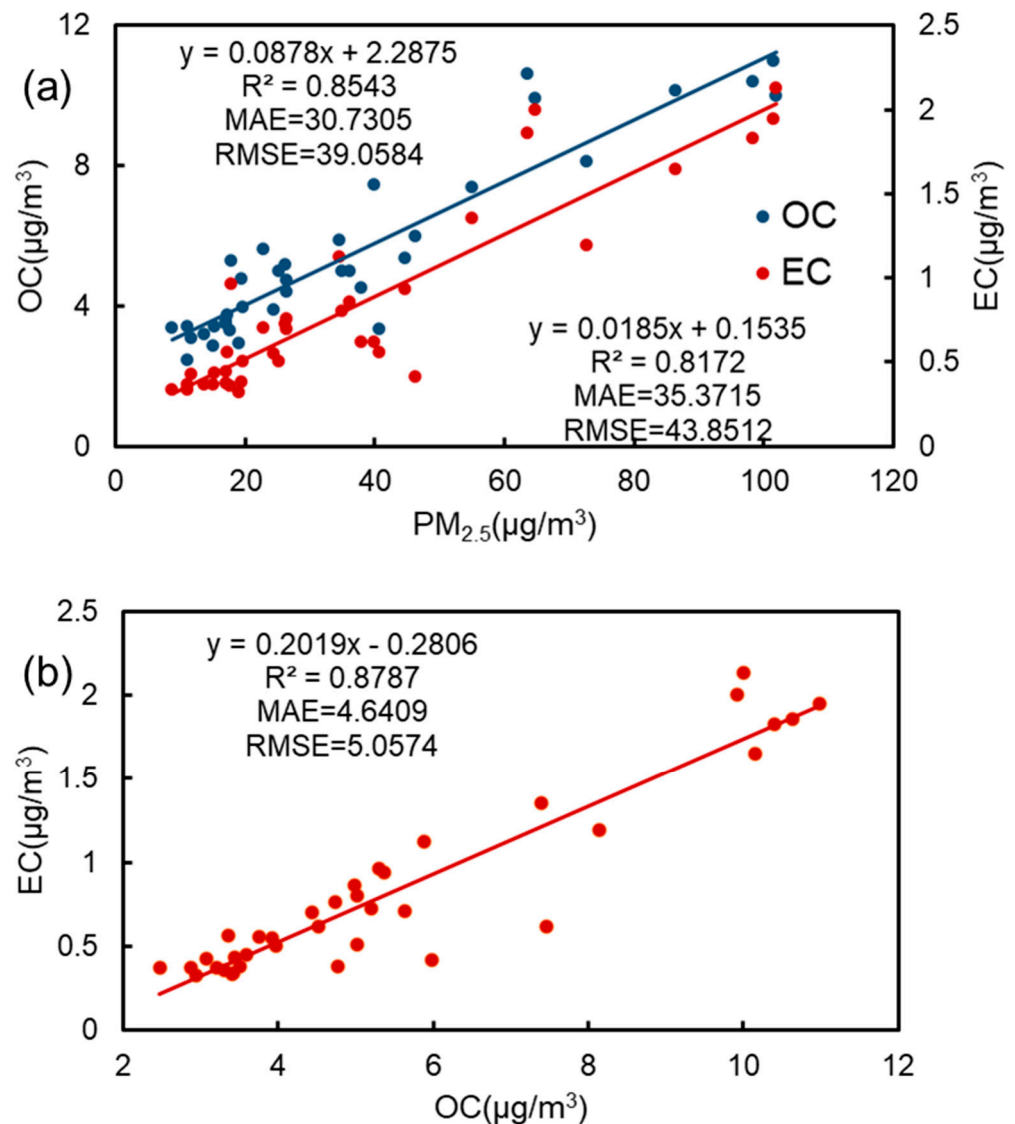


**Figure 2.** (a) shows the correlation of  $PM_{2.5}$  with OC and with EC. (b) is the correlation of OC and EC.

We calculated the average concentration in three time periods for  $PM_{2.5}$ , OC, and EC. During the control period, three species all showed the lowest level (Figure 1b). The average concentrations for the “during” period of the three species are 21.96, 3.92, and  $0.49 \mu\text{g}/\text{m}^3$ , whereas in the “before” period they are 54.37, 7.48, and  $1.18 \mu\text{g}/\text{m}^3$ .  $PM_{2.5}$  reduced 64.55% in the “during” period and increased over 104.0% after the control period. OC and EC also both showed a large reduction during the control period. The reduction rates for OC and EC are 48.74% and 60.75% and both species increased by 70.48% and 130.24% after the control period compared to the “during” period. The EC species and  $PM_{2.5}$  showed the largest reduction rate and EC even showed the largest increase rate after the control period. These evident reduction rates are mainly the results of emission reduction of certain sources like organic matter, transportation, power, and industry. Those are major sources in the mid-south region of Hebei Province, which is traditionally the source region for Beijing [9,37]. Those sources tend to contribute the most to primary atmospheric pollutants in the BTH region and possibly be the core reason for the relatively high concentration in non-control periods.

Other airborne compounds CO,  $\text{NO}_2$ , and  $\text{SO}_2$  all showed the same trends as with  $PM_{2.5}$  and organic matter (Figure 3). CO and  $\text{SO}_2$  are both inorganic tracers for emission sources containing fossil fuels burning. These sources majorly include pollution depart-

ments of industry, power, and minor transportation.  $\text{NO}_2$  was mainly contributed by transportation sources and a few by other fossil fuel burning sources. These three sources were largely constrained during the control period and the emission pollutants were reduced significantly and lead to the reduction of CO,  $\text{NO}_2$ , and  $\text{SO}_2$ . After the control period, the emission level from these three major sources would increase in a short period, but the chemical production reaction speeds of specific compounds would differ. This led to the relatively low increase rate with CO in the “after” period, and CO mainly comes from incomplete combustion processes of carbon-related emission sources. The concentration level of  $\text{NO}_2$  and  $\text{SO}_2$  both got higher in the “after” period compared to the “before” period. This further indicated that the contribution to CO from industry and power sources should be lower than that in  $\text{SO}_2$ .

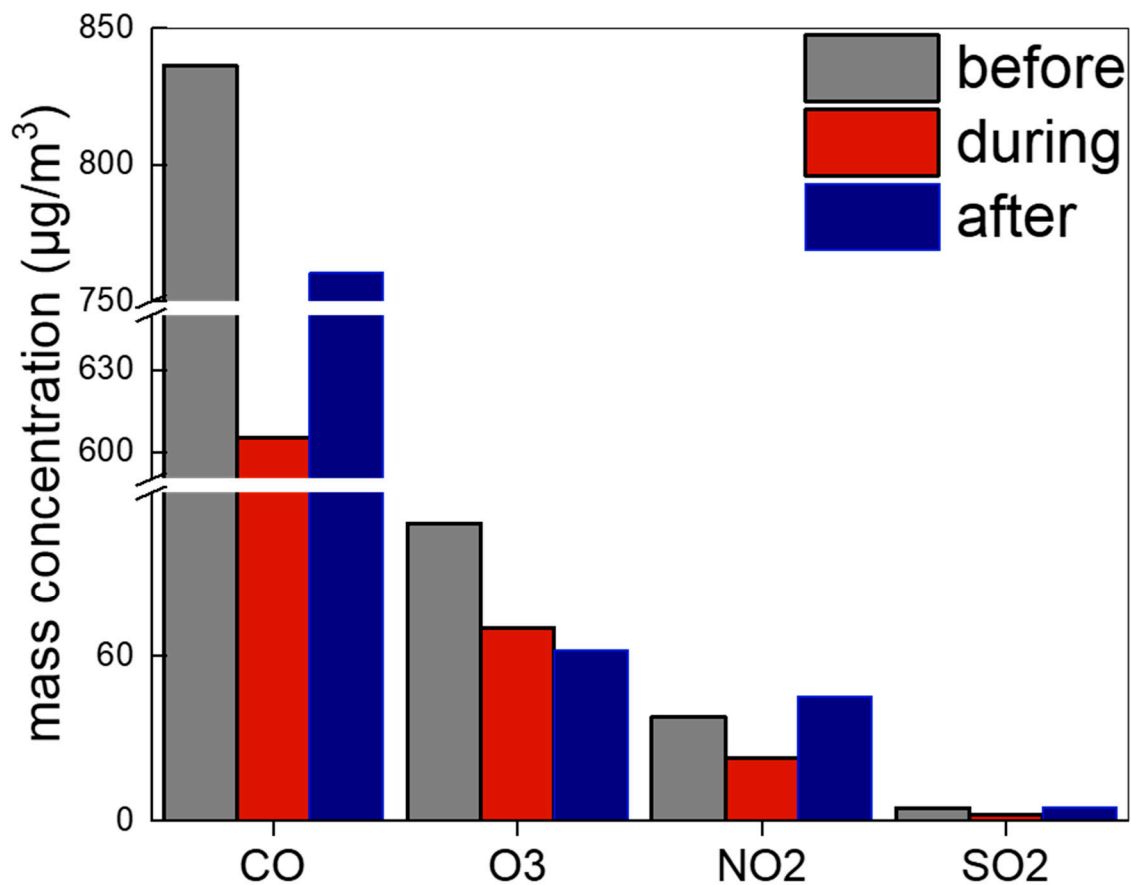


**Figure 3.** The column plots for other atmospheric chemical compound concentration in three periods (CO, O<sub>3</sub>, NO<sub>2</sub>, SO<sub>2</sub>).

For O<sub>3</sub>, the results showed opposite trend compared to other three compounds (Figure 3). The “after” period of O<sub>3</sub> showed the lowest concentration level. This could be the result of the production reactions of O<sub>3</sub> in the atmosphere and the large increase of NO<sub>2</sub> and other VOCs in non-control periods. The increase of NO<sub>2</sub> and other VOCs resulted from the release of fossil fuel burning sources in the BTH region. Pollutants from these sources are normally primary emissions and increase NO<sub>2</sub> and other VOCs at a faster speed and this status puts O<sub>3</sub> in a rather constrained concentration level. As a result, O<sub>3</sub> was reduced after the control period while NO<sub>2</sub> was increased instead and it would take a certain amount of time for O<sub>3</sub> to increase to the “before” period concentration level. This indicated reverse trends of O<sub>3</sub> and NO<sub>2</sub> in certain air quality control periods and this should be part of the EMKA curve approach in the VOC high concentration area [38,39]. At this point of the timeline, the reduction of VOCs from transportation source and NO<sub>x</sub> emitted from industry and power were experiencing different reduction percentages. These

evident trends of NO<sub>x</sub>, VOCs, O<sub>3</sub>, and related reduction of emission variations can be used to modify the mechanism in atmospheric chemistry and can be coupled in atmospheric numeric models.

The correlations values (R) between PM<sub>2.5</sub>, SO<sub>2</sub>, CO, NO<sub>2</sub>, O<sub>3</sub>, OC, and EC also indicated the potential contribution of different sources (Table 1). The lowest correlation value was between O<sub>3</sub> and NO<sub>2</sub> with only 0.15. Considering the containment reactions of NO<sub>2</sub> and VOCs producing O<sub>3</sub> and the massive possible emission of VOCs and NO<sub>x</sub> in the BTH area from transportation, this feature should be reasonable under significant emission reduction periods. In addition, the correlations between O<sub>3</sub> and the other five species were the lowest on average. The corresponding R-values with PM<sub>2.5</sub> was 0.66 (Figure 4d), with SO<sub>2</sub> was 0.48, with CO was 0.52, with OC was 0.67, and 0.57 with EC. This was also in accordance with the feature that O<sub>3</sub> showed the opposite trends against other species, which shows how O<sub>3</sub> could have different production mechanisms on a regional scale in northern China. On the other hand, although there may be great differences between the sources of O<sub>3</sub> and other species, especially PM<sub>2.5</sub>, OC, and EC, the overall correlation is relatively significant, especially the correlation with PM<sub>2.5</sub> and OC, which may be due to the fact that O<sub>3</sub> and PM<sub>2.5</sub> are restricted by meteorological conditions and external transport to some extent. Apart from O<sub>3</sub>, the other five species all showed R-values over 0.6 with each other. The correlations between PM<sub>2.5</sub>, OC, and EC showed R-values all over 0.9 and were among the highest in all the R-values results, and the R-value between OC and EC was the highest with 0.94. This was showing the closest relationship of organic matter and PM<sub>2.5</sub> in the BTH region and corresponding organic matter sources should be the largest contributor in this area, especially primary organic matter sources. At the same time, PM<sub>2.5</sub> showed relatively high R values with SO<sub>2</sub> (0.85) and CO (0.88) but with a lower correlation with NO<sub>2</sub> (0.69) (Figure 4a–c). The coal-burning sources could be contributing more to PM<sub>2.5</sub> than transportation source to some extent. Apart from those above, we can also see other relatively high R-values over 0.8 between SO<sub>2</sub> and OC (0.86), SO<sub>2</sub> and EC (0.87), CO and OC (0.80), and CO and EC (0.85). These species were all highly contributed from sulfur and carbon emission sources. There are many overlaps between both sources in the BTH area, such as power plants, industrial factories, and partially from straw burnings (biomass burning). Those major fossil fuel combustion emissions sources are still considered to be one of the largest sources in the BTH region, which is evidently consistent with existing findings [18] and are the main reduction targets of the temporary air quality control policies from the governments. During the control period, these sources and related compounds such as organic matter species should be reduced significantly. Since these compounds were showing evident correlations and features along or against each other, future studies should be focused on deep mechanisms and coupled reactions of gaseous atmospheric compounds and corresponding contributions to PM<sub>2.5</sub>.

**Table 1.** Correlation value (R) between PM<sub>2.5</sub>, SO<sub>2</sub>, CO, NO<sub>2</sub>, O<sub>3</sub>, OC, and EC. Data with a green background are R values greater than 0.8. The yellow background are R values less than 0.6. The crimson background are R values between 0.6 and 0.8.

	PM <sub>2.5</sub>					
SO <sub>2</sub>	0.85					
CO	0.88	0.74				
NO <sub>2</sub>	0.69	0.80	0.59			
O <sub>3</sub>	0.66	0.48	0.52	0.15		
OC	0.92	0.86	0.80	0.70	0.67	
EC	0.90	0.87	0.85	0.74	0.57	0.94

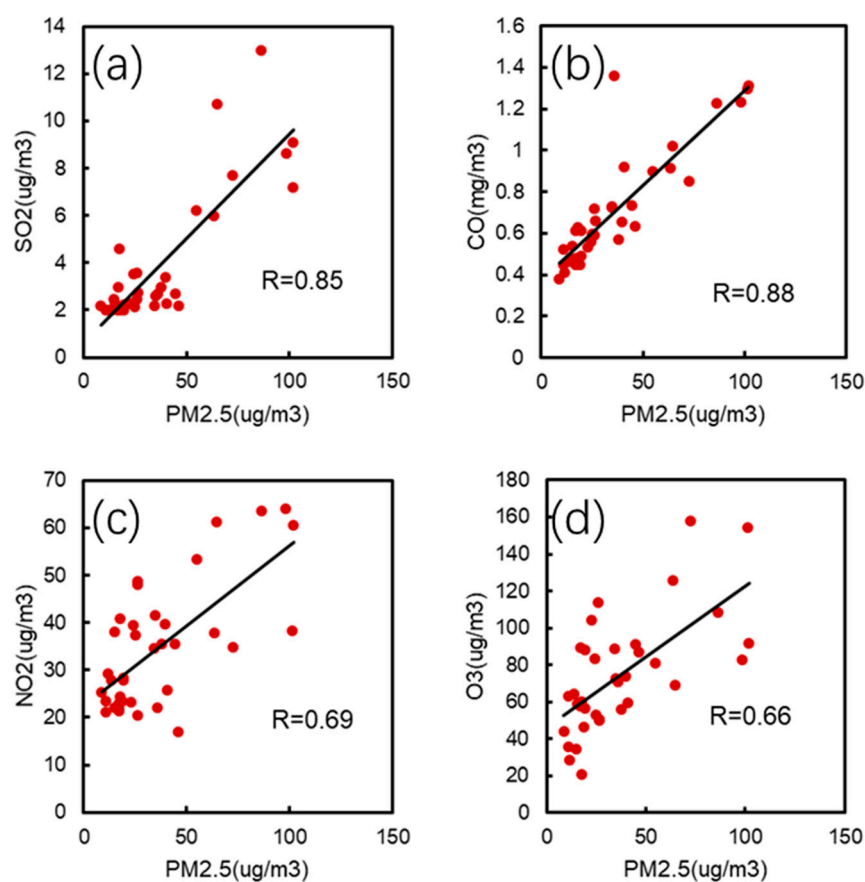


**Figure 4.** Plots (a–d), respectively, show the correlation graph array between  $PM_{2.5}$  and  $SO_2$ , CO,  $NO_2$ , and  $O_3$ . The correlation coefficient R values are given in the subplots, respectively.

### 3.2. Primary and Secondary OC

POC and SOC both showed reduction during the control period but SOC reduced after the control period whereas POC increased at the same trend as  $PM_{2.5}$  and OC (Figure 5). The average concentrations of SOC in the three periods are 1.96, 1.62, and 1.43  $\mu\text{g}/\text{m}^3$  while the concentrations of POC are 5.52, 2.30, and 4.64  $\mu\text{g}/\text{m}^3$ . POC showed the lowest concentration during the control period. The reduction rate was 58% in the “during” period and increased by 102% after the control period. The SOC, on the other hand, reduced only 18% during the control period and also reduced 12% after the control period. The atmospheric chemical chain reactions producing SOC should take a certain amount of time to increase to the emission level changes whereas the POC could react much faster to the emission variations. The reduction rate of SOC during the control period was also evidently lower than the POC, which is consistent with the trends of OC and EC. Most primary atmospheric compounds should be more sensitive than secondary compounds, including some  $PM_{2.5}$  chemical components. This phenomenon is also consistent with the major primary emission sources and corresponding emission levels in the BTH region [11,14,15]. For some short periods, the temporary air quality guarantee measures may not show some direct reduction impact or at least the correct reduction level because of the lag effects.

### 3.3. Organic Matter Species

We selected three representative organic matter species types to discuss the variation of major organic matter sources in three time periods. The three organic matter species contains aldehydes, alkanols, and sterols. Each category contains four specific species. Syringaldehyde, 4-hydroxy-3-methoxycinnamaldehyde, vanillin, and nonyl aldehyde are the aldehydes category. Glycerine, tricosanol, eicosanol, and triacontanol for alkanols.

Cholestanol, sitosterol, stigmasterol, and campesterol for sterols. Despite the three categories are all secondary organic matter, they all showed the same trends no matter on the whole category or for individual species. The average concentration all reached the lowest in the “during” period while reduction and increase were detected in the “before” and “after” periods (Figure 6, Table 2), respectively.

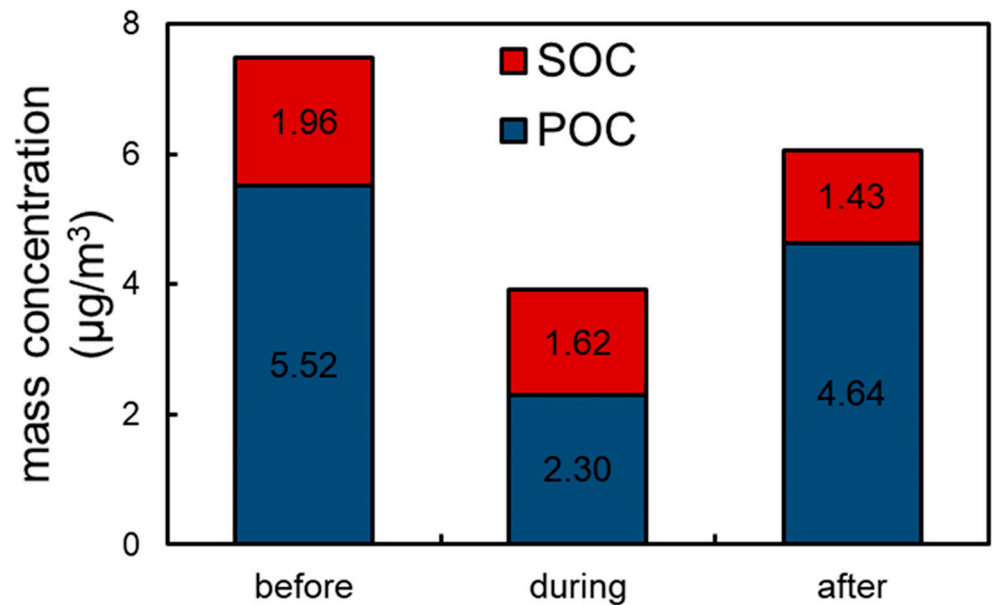


Figure 5. Concentration of SOC and POC in 3 periods. The average concentrations are marked inside the columns.

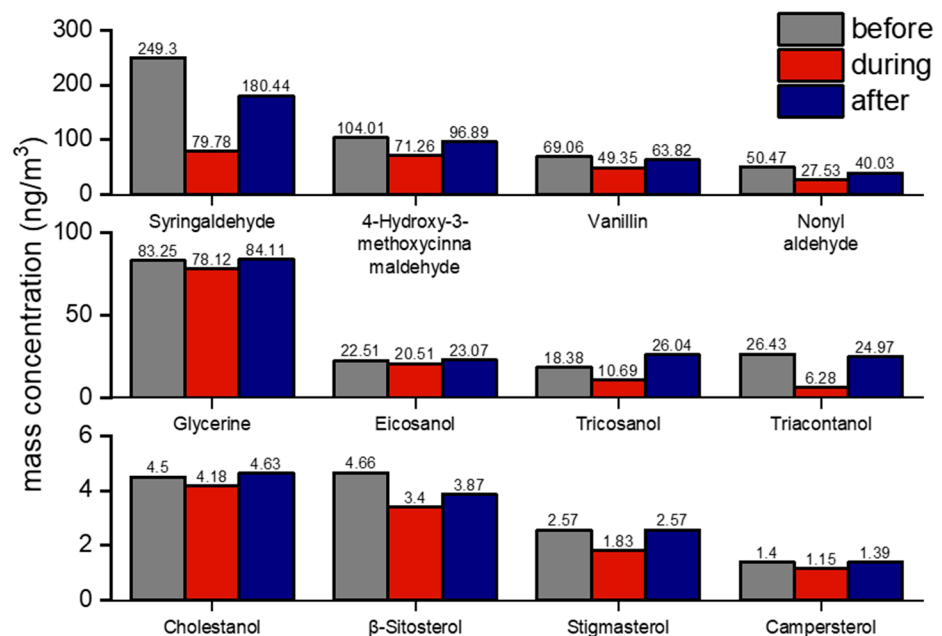


Figure 6. Average concentrations for aldehydes, alkanols, and sterols categories in three time periods. The concentration data are marked on the column bars.

**Table 2.** Total average concentration of aldehydes, alkanols, and sterols in three time periods (ng/m<sup>3</sup>).

	Aldehydes	Alkanols	Sterols
before	472.84	150.57	13.13
during	227.91	115.59	10.55
after	381.19	158.19	12.47

For aldehydes, syringaldehyde, 4-hydroxy-3-methoxycinnamaldehyde, and vanillin are all considered tracers for biomass burning sources [26,40–42]. This could be due to the massive agriculture burning of straws during the autumn harvest season in the BTH region. These agricultural fields are spread over most southern Hebei Province area. At the same time, nonyl aldehyde can be the organic tracer for residential cooking activities in the BTH area [26,40–42]. The reduction rate in the “during” period of syringaldehyde, 4-hydroxy-3-methoxycinnamaldehyde, and vanillin are 68.0%, 31.49%, and 28.54% whereas their increase rates are 126.18%, 35.97%, and 29.34%. The largest rates from syringaldehyde could be due to the major contribution from biomass burning sources. This would be the reason syringaldehyde was more affected by the emission variation than other aldehydes species. The reduction and increase rates of nonyl aldehyde were 45.45% and 45.41%, which would be evident that residential emission level changed largely in three time periods separately. Compared to 4-hydroxy-3-methoxycinnamaldehyde and vanillin, nonyl aldehyde are also mainly contributed by cooking sources, which were changing significantly during the control period. Showing that biomass-burning and cooking sources shared the same changing extents in three periods. These two sources are mainly located in rural and urban areas but the emission amount or variation level may be the same in BTH region. This could be part of future related emission inventory researches.

For the alkanols category, tricosanol and triacontanol are considered to be tracers of coal-burning while glycerine and eicosanol are considered to be tracers of oil burning and partially biomass burning [26,40–43]. It is reasonable that we took the alkanols category as tracers for main fossil fuel burning sources. Separately, tricosanol and triacontanol are showing larger reductions and increase percentage than glycerine and eicosanol, which is highly in accordance with the emission variation of coal burning and oil burning. Specifically, the reduction rates of the two coal-burning tracers are 41.85% and 76.25% while the oil-burning tracers only showed 6.16% and 8.88% reductions in the “during” period. The increase rates are 143.59% and 297.83% for the coal-burning tracers after the control period while the oil-burning tracers are only 7.67% and 12.49%. This huge gap between potential coal burning and oil burning emission variations indicated that coal burning is contributing much more than oil burning in the BTH region [43]. This is implying that the emission from power plants, common industry factories, and possible minor residential are holding a larger contribution to PM<sub>2.5</sub> than the oil-burning sources with transportation and a few power emissions. Industry and power plant departments were experiencing higher reduction during the control period than transportation departments, which led to moderate differences of these two types of fossil fuel burning sources in the whole sampling period.

Among the four sterol species, cholestanol is considered the only tracer of cooking sources in the city area, which can be a part of the residential emission department. The other three species  $\beta$ -sitosterol, stigmasterol, and campesterol are all considered as biomass burning organic tracers [26,40–42]. The entire sterols category showed the smallest concentration level in the OC scope. The average concentrations of the three periods were only 13.13, 10.55, and 12.47 ng/m<sup>3</sup>. Furthermore, these four species all showed a reduction rate below 30% while the aldehyde species with the same tracer features showed a reduction rate over 28%. Indicating the minor contribution from sterols category species to organic matter and PM<sub>2.5</sub> in the BTH region, corresponding to their concentration levels. This led to the result that PM<sub>2.5</sub> and OC should be less influenced by the variation of sterols species given the relatively minor contributions. Specifically, cholestanol showed the lowest reduction and increase rate in the “before” and “after” periods, which indi-

cated that the contribution from residential cooking to sterols species did not reduce as much as the contribution to aldehydes species, not to speak about fossil fuels combustion sources, while biomass burning can make a difference in certain scenarios. Thus, there can be major biomass burning emission during the Summer–Autumn period and minor cooking emission in the BTH region. Cooking emission could be least affected by other air quality control policies. This is to some extent contrary to the previous alkanols discussions about biomass burning and cooking sources, which should be the difference in specific contribution pollutants from these two sources.

### 3.4. Model Results

We evaluated the simulation performance of meteorological parameters simulated by the WRF model. The meteorological parameters include temperature, wind speed, and dew point temperature (Table 3). The simulation performance of the three parameters was generally good and can be basically used for a FLEXPART model trajectory simulation calculation. The temperature simulation was the best, with a correlation value of 0.88 and RMSE 5.36. The observed values of wind speed were basically consistent with the average simulated value, with their mean value of 2.31 and 3.67, respectively. The correlation coefficients were 0.47 and RMSE is 2.12. The difference between the observed dew point temperature and the simulated value was relatively large, but the correlation coefficient was 0.46. The simulation results were consistent with the observed values in trend.

**Table 3.** WRF simulation performance assessments. OM represents observation mean value. SM represents simulation mean value. R represents the Pearson correlation value. RMSE represents Root Mean Squared Error and MAE represents mean absolute error.

	Temperature	Wind Speed	Dew Point Temperature
OM	23.82	2.31	16.62
SM	28.85	3.67	8.33
R	0.88	0.47	0.46
RMSE	5.36	2.12	9.01
MAE	5.04	1.58	8.64

For the new post-processing Lagrangian model method, the RTA results represent the transport trajectories plume features with particles. The RTAs in three time periods showed a large difference in time order (Figure 7a–d) and the sampling site showed clear long-range transboundary transport influence during the whole sampling period. Before the control period, Beijing was dominantly impacted by long-range southwestern transboundary transport path. The farthest potential air mass source region could be the mid-southern area of Hebei Province, which has been a major source area of industry, power, residential, and agricultural emissions [13,14,24]. During the control period, the wholesome air mass transboundary transport features changed to another direction, which is the northeast long-range area in Hebei Province. This whole air mass plume covered half of the northeastern area in Hebei Province, mostly Chengde and Zhangjiakou cities. Chengde city and Zhangjiakou city have been marked as the ecological conservation area according to the development plan from the government of Hebei Province [44]. The northern Hebei Province area is not considered a primary atmospheric pollutants source region. Thus, this path accumulated a relatively small amount of air pollutants during the control period because of the control policies and these emissions were contributing to Beijing city. After the control period, the long-range transboundary transport features changed back to the status before the control period. The potential air mass source region also altered back to the mid-south cities in Hebei Province. In the RTA fields of the whole sampling period, these two evident transboundary transport paths almost share the same path length and these two paths shared the same air mass transport intensity. Our wind direction rosettes (Figure 8) also largely validate this transmission channel feature. Especially in the “before” (Figure 8a) and “during” (Figure 8b) stages, the frequency of

the opposite direction of the wind directions appear to be very different during these two periods. The incoming wind direction from the southwest was the dominant wind direction before the control period (frequency 65). During the control period (frequency 92), the wind rapidly changed to the characteristic of coming from the northeast direction. However, a small number of incoming winds from direct south and east appeared before and during the control period. However, the frequency was about half of the dominant southwest and northeast wind direction, respectively. These two directions also correspond to the key emission source area and relatively clean area of Hebei province, respectively. After the control period (Figure 8c), the dominant wind direction showed some differences. The most frequent incoming wind direction is still southwest (frequency 79). Meanwhile, the incoming wind frequency in the south direction (frequency 78) is the same as that in the southwest direction. This is also consistent with the pre-control characteristics. However, different from the “during” period, relatively significant incoming winds from east and northeast also appeared after the control period, and the frequency of both of them are the same (frequency 56). In the overall wind direction chart (Figure 8d), the frequency of incoming wind from southwest and northeast is basically the same (164 and 169, respectively), and the frequency of south direction also reached 145. Considering the longer non-control period, the northeastern transport path should have much fewer impacts on accumulating atmospheric pollutants. Additionally, the air quality control policies may prove less necessary in the northern Hebei region. In addition to the analysis of the meteorological system during the overall study period, we also analyzed two significant high  $PM_{2.5}$  concentration periods (Figure 8e,f). Two periods of high value occurred around 16–17 August and 16–17 September, respectively. The dominant wind direction in the two pollution periods was obviously pointing to the southwest channel. In the first process, there was also a significant wind direction transmitted from due south, while in the second process, the wind frequency from the northeast direction was second only to the southwest direction. This can also explain the key role of the Southwest Passage in the transport of air pollutants to Beijing.

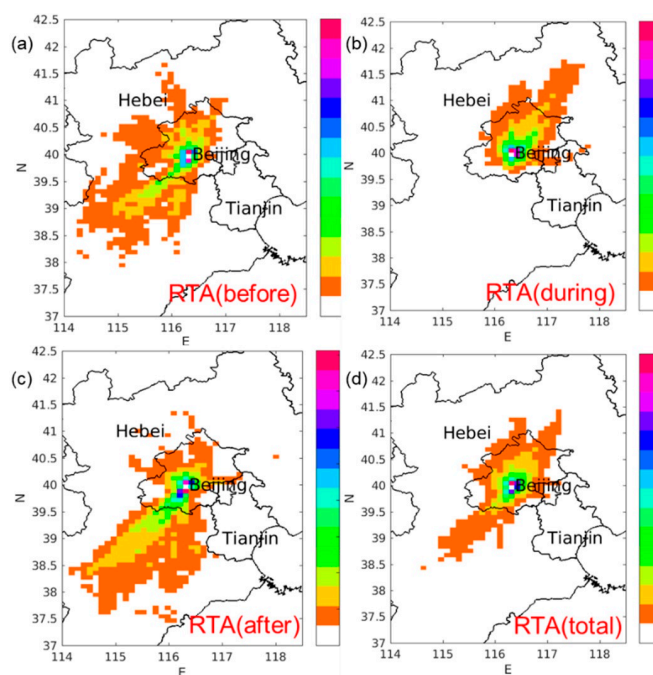


**Figure 7.** RTAs of the 3 time periods and the whole sampling period. Subplots (a–c) are the RTA fields for the “before”, “during”, and “after” periods. Subplot (d) is the whole sampling period. The red dot is our sampling site and the particle release point in FLEXPART model. The color bar represents the relative contribution percentage in each grid to the sampling site. From bottom to top side of the color bar, the cell contribution gets higher.

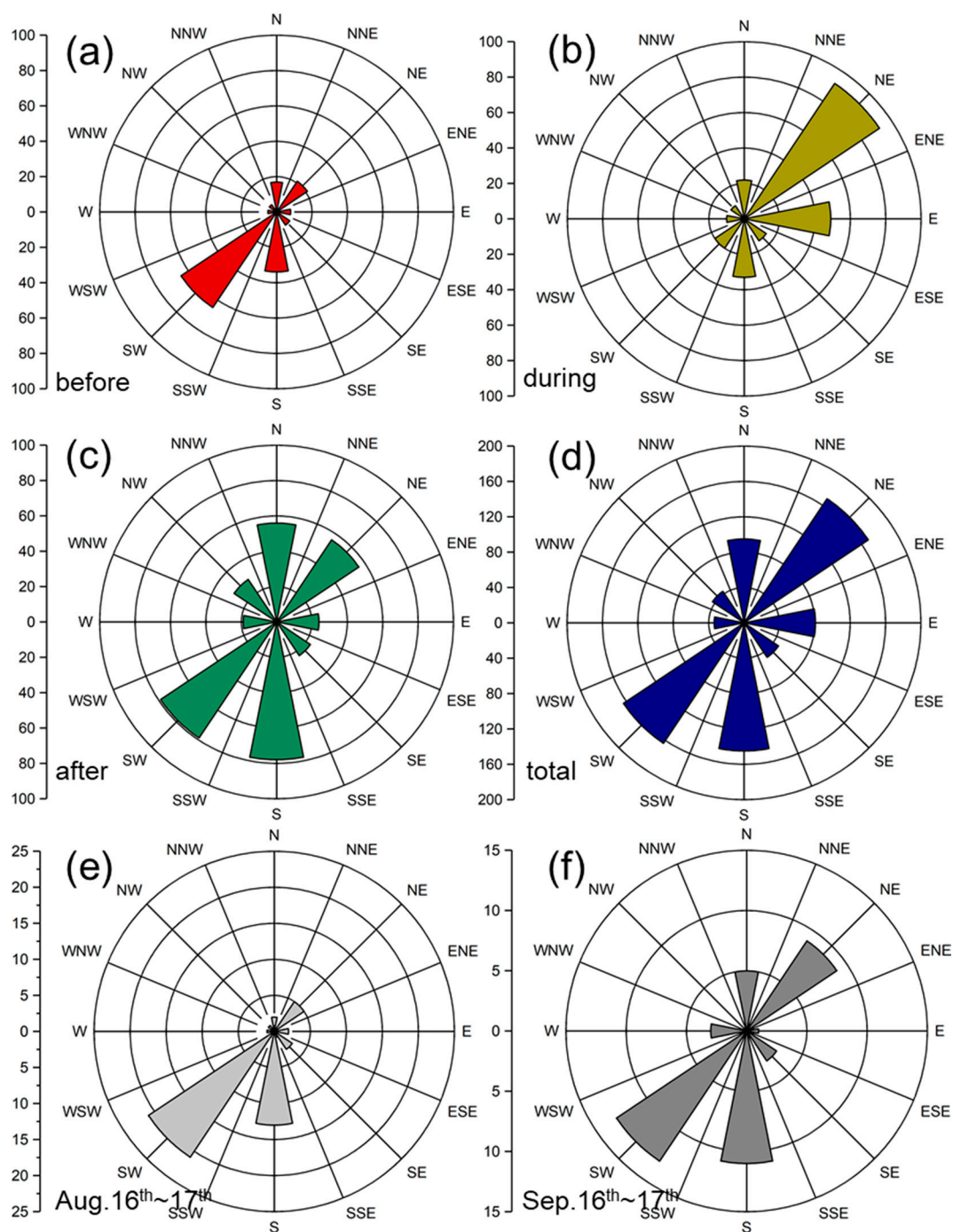


**Figure 8.** Wind rose plots of the three separate periods and the total sampling period. The (a–c) subplots are for the before, during, and after periods. The total wind rose plot is the subplot (d). The same scale is used for wind direction frequencies in the three periods. The data used in this plot are hourly instantaneous data from the China National Air Pollution Control Monitoring System. Subplots (e,f) are the wind rose plots for two separate PM<sub>2.5</sub> high concentration periods: 16–17 August, 16–17 September.

For the CFA results from model simulations, the CFA fields for PM<sub>2.5</sub>, OC, and EC in three periods shared almost the same trends (Figure 9a–d, and Figures S1 and S2 from Supplementary Materials), separately. Additionally, the other three gaseous compounds CO, NO<sub>2</sub>, and SO<sub>2</sub> also showed almost the same transport patterns with PM<sub>2.5</sub> (S3 from Supplementary Materials). The dominant transboundary transport channel was the southwest direction away from the Beijing domain in non-control periods, and the

potential source region was mostly from the south and middle parts of Hebei Province. These potential contributing channels all appeared out of the control period and showed evident high concentration data of  $PM_{2.5}$ , gaseous compounds, and organic matter. The southern and middle Hebei province are in fact potential atmospheric pollutants emission sources, and mostly include primary emissions, power, industry, and transportation sources. These sources are mostly related to carbon compounds, sulfide, and oxynitride in the BTH region. However, these potential source regions did not impact the air quality in the Beijing area during the control period, whereas the potential source region during the control period was the northeast area and cities, mostly Chengde city as assumed in the RTA results discussion. Considering the evidently lower  $PM_{2.5}$  and pollutants concentration data in the “during” period, the accurate contribution amount of atmospheric pollutants from Chengde city area should be much lower than the southwest path region, indicating that the air quality control policy carried out in southern Hebei cities did not contribute significantly to the pollutants concentration reduction in Beijing city. The meteorological conditions, including long-range wind movements with a much lower concentration background from the northeast direction, largely dispersed the existing  $PM_{2.5}$  and organic matter in Beijing city.

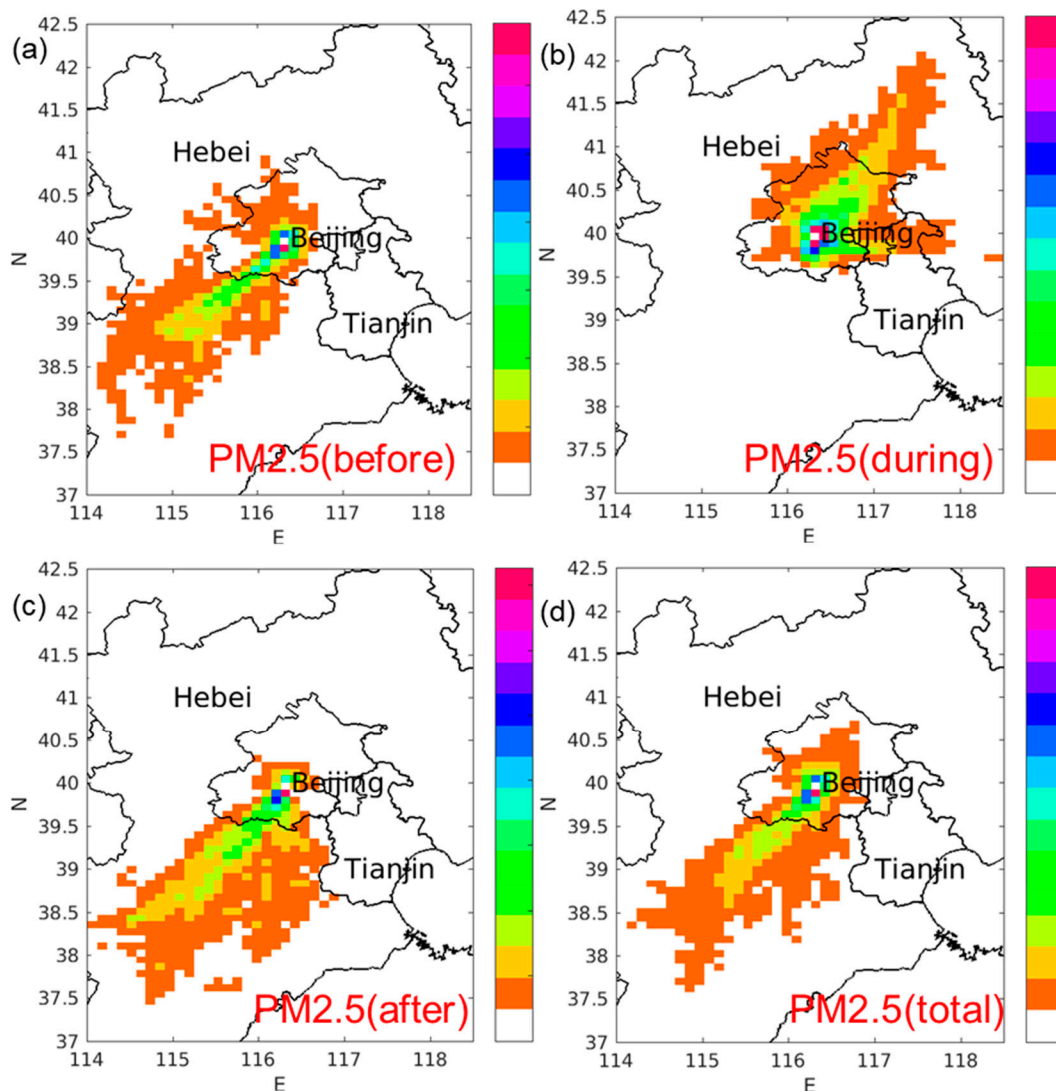


**Figure 9.** CFA fields plots of  $PM_{2.5}$ , OC, and EC in 3 time periods. Subplots (a–d) are CFAs of  $PM_{2.5}$  in 3 time periods and the whole sampling period, respectively. The red dot is the sampling site and particle release point in FLEXPART. The color bar only represents the relative contribution percentage in each grid. Beijing city, Tianjin city, and Hebei Province are marked in the maps. From bottom to top side of the color bar, the cell contribution gets higher.

By further taking advantage of the RTA and CFA plots, we calculated the contribution percentage from the two major transboundary transport channels to the Beijing area (Table 4). The contribution percentage features followed the same patterns for PM<sub>2.5</sub>, OC, and EC. The contribution from southwest transport path was all over 40% before the control period and the contribution to PM<sub>2.5</sub> even reached up to over 50%. After the control period, the southwest path contributed roughly 60% to Beijing domain and there were no other significant long transboundary paths. This completely confirmed the qualitative assumption in the previous CFA discussion that the southeast path was the dominant contribution of PM<sub>2.5</sub> to Beijing during the non-control period. During the control period, the contribution from the northeast path was over 60% but with significantly low PM<sub>2.5</sub> and OC concentration, given the average concentration level we had in Figure 1b. EC also showed a 54.68% contribution from the northeast path during the control period. The over 40% contribution from the southwest path lead to the high concentration during the non-control period and this path did not show significant transport area and contribution to Beijing city during the control period from the CFA subplots. Instead, the relatively “cleaner” northwest path transported “cleaner” air mass to the Beijing area even though this channel contributed the most to Beijing city. Last but not the least, other transport paths only covered roughly 40% OC and EC to Beijing and only 34.79% for PM<sub>2.5</sub> including minor transport from the northeast path, confirming that the definite contribution level of southwest should outweigh a lot more than the northeast path on a normal emission level.

**Table 4.** Contribution percentage (%) of long-range transport paths. SW represents the southeast path. NE represents the northeast path. Others contains all not significant transport contribution. Local represents the transport within Beijing domain. The total column represents the whole sampling period. Only significant transport paths in CFA fields were calculated.

		Total	Before	During	After
PM <sub>2.5</sub>	SW	52.7	52.57	-	68.56
	NE	-	-	60.54	-
	others	34.79	35.69	18.42	21.79
	local	12.51	11.74	21.04	9.65
OC	SW	42.39	43.87	-	59.19
	NE	-	-	62.66	-
	others	43.47	40.53	12.56	29.39
	local	14.14	15.60	24.78	11.42
EC	SW	44.11	43.01	-	59.58
	NE	-	-	54.68	-
	others	40.64	41.11	20.58	27.35
	local	15.25	15.88	24.74	11.07

The RTA and CFA results from parallel cases of 2014 and 2016 showed quite different transport patterns in both years (Figures 10 and 11). At the same time, the transboundary transport results took evident patterns that can explain the source emission region and were mirrored by our previous conclusions.

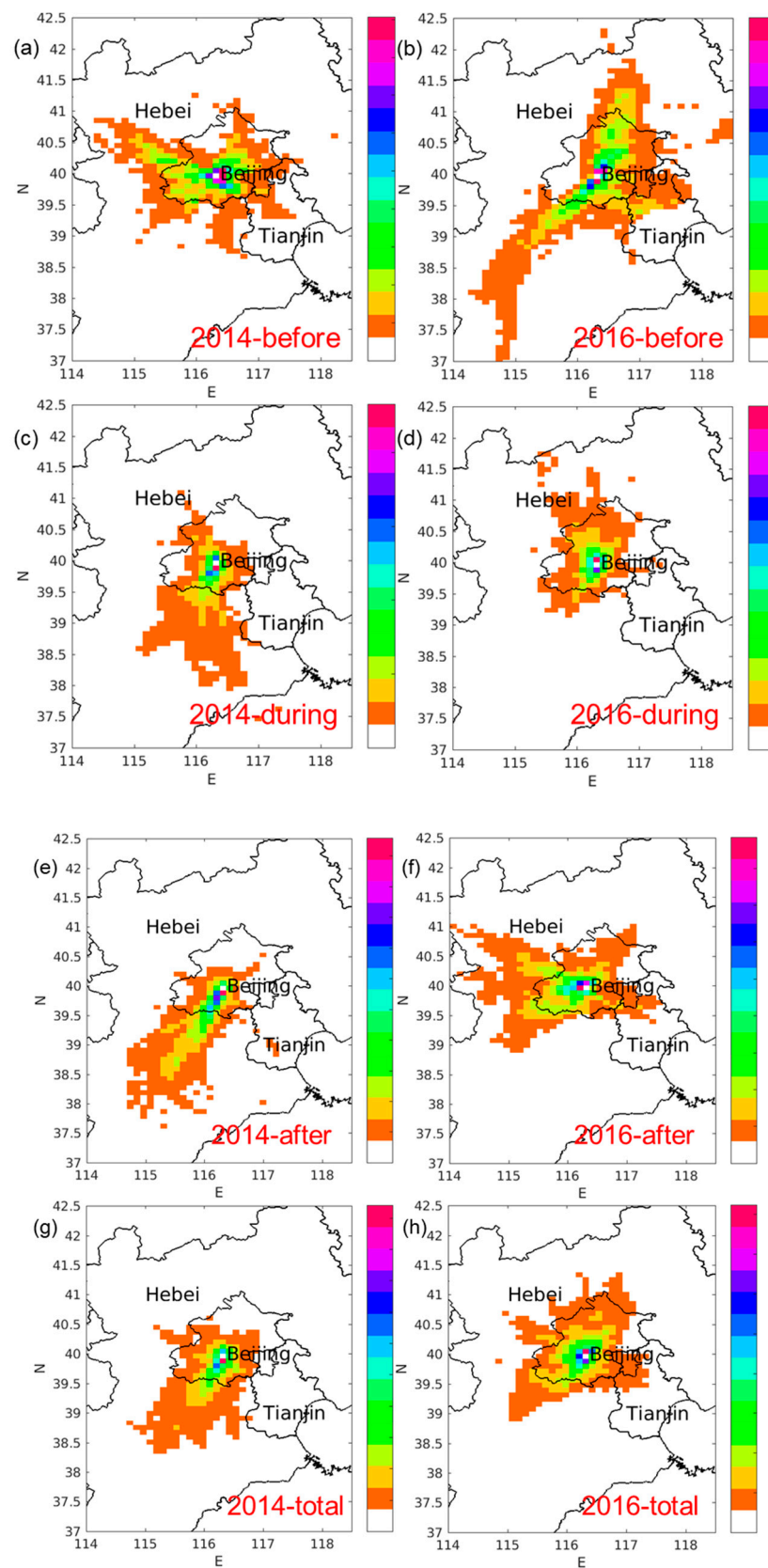


**Figure 10.** RTAs of four time periods (before, during, after, total) in 2014 and 2016. Subplots (a,c,e,g) are for the year of 2014 and (b,d,f,h) are for the year of 2016. From bottom to top side of the color bar, the cell contribution gets higher.

In the year 2014, the “during” and “after” periods almost showed the same air mass transport patterns (Figure 10a,c,e,g). In these two periods, the southwestern path was the dominant transport path, and some related cities like Baoding, Langfang, Shijiazhuang, and Xingtai became the air mass source region, while the “before” period showed massive short-range transport and local regions was the dominant air mass source region. In the “before” period, most of the Beijing city area contributed air mass significantly to the Olympic park site, and only some surrounding counties in Tianjin, Zhangjiakou, Baoding, and Langfang city contributed to the monitoring site. However, the “total” RTA (Figure 10g) result in 2014 only presented prominent southwestern transport path just the same as the “before” and “after” periods in 2015. Showing that although the surrounding Beijing area contributed air mass to the Olympic Park site, the southwestern path was the dominant transport channel at the same period in 2014, holding significantly more air mass density and frequency. Which are the same as the year 2015 to some extent. Additionally, in 2016, the transport patterns altered evidently in three periods and the whole research period (Figure 10b,d,f,h). The overall transport pattern was mainly concentrated on Beijing city. Most Beijing area was the dominant air mass source region. Only a part of Tianjin, Baoding, Zhangjiakou, and Chengde city contributed air mass to the monitoring site, most of which were located in the surrounding area of Beijing city. In the 2016 case, only the “before” period (Figure 10b) showed noteworthy long-range transboundary transport from both the southwestern and northeastern paths. However, the southwestern path still outweighed the other path on air mass contribution and transport distance. Indicating the stronger density and frequency of southwestern path transport, which also agreed with some previous conclusions. For the “during” and “after” periods in 2016 (Figure 10d,f), the air mass transport patterns mainly focused on the Beijing city area and some of the surrounding counties in Hebei Province and Tianjin city. However, the contribution area got much wider in the “after” period, and the “during” period showed that almost the whole Beijing area was the air mass contribution region. Therefore, the total RTA result of 2016 was more like the compromise of southwestern path, northeastern path, surrounding area, and Beijing city itself. The PM<sub>2.5</sub> CFA results of 2014 and 2016 were mostly inconsistent with the RTA results (Figure 11a–h) except for some minor offsets in the year 2016. These noticeable offsets are mostly located in some western and southern regions. However, the CFA results themselves could not help getting any conclusions on the emission level in the BTH region except for confirming some potential regions. However, analyzing the PM<sub>2.5</sub> average concentration results (Figure 12) in three periods of the three years reached some conclusions. The year 2016 showed almost the same trend as the year 2015 even though there were no remarkable air quality control measures, but the reduction and increase percentages of “during” and “after” periods were much lower than 2015. The average concentrations for the total period in 2015 and 2016 are 36.89 and 38.14  $\mu\text{g}/\text{m}^3$ . Considering the existence of national air quality control policies and other regional government measures, proper concentration reduction could be due to the emission reduction. If without the temporary control policies in 2015 during the celebration events, the concentration should be remarkably higher than the 2016 concentration level. Showing that the variations in 2016 could only be the result of the long-term regional control measures. To further confirm this assumption, the total average concentration of 2014 was much higher than the other two years with 66.43  $\mu\text{g}/\text{m}^3$ . Moreover, 2014 also showed different variation trends in three periods with their higher concentration levels in time order. This feature along with our CFA results (Figure 11a–h) would help us confirmedly identify the potential source region in the BTH area. In 2014, the southwestern transport path was the dominant channel in the “after” period and was almost the dominant path in the “during” period, but the density was reduced and biased to the eastern area in Hebei Province. In the “before” period, the model did not present evident transport from southern cities which were believed to be major emission sources so the “before” period remained the lowest concentration level. This led to the PM<sub>2.5</sub> uprising concentration trend in three periods in the year 2014 and the meteorological conditions clearly avoided the transport of atmospheric pollutants from southern Hebei

cities in the “before” period. In the same period in 2016, both the “before” and “after” periods showed significant long-range  $PM_{2.5}$  transport from southwestern, northeastern, and western Hebei Province and partially northern Tianjin city, which are considered massive emission source regions. The “during” period (Figure 11d) however, showed that most of the  $PM_{2.5}$  contribution region was from Beijing city itself. It is reasonable to conclude that the reduction of long-range Hebei and Tianjin contribution region in the “during” period reduced the  $PM_{2.5}$  concentration level. Even though Beijing city kept nonnegligible  $PM_{2.5}$  emission amount mostly from transportation and residential sources, the reduction of outside circumjacent major source region still showed some effects in reducing Beijing’s local  $PM_{2.5}$  concentration to a certain extent. For the 2014 case, the southwestern channel was the only considerable long-range path for the whole investigation period (Figures 10g and 11g). Even if taking the national and local air quality control policies and the reduction effects into consideration, the southwestern channel still contributed the most to the Beijing area during this Summer–Autumn season. The special and altering meteorological conditions in this area helped prevent some major emissions transported to the Beijing area regardless of the existence of major emission source region from Baoding, Shijiazhuang, and Langfang city. Regrettably, the air mass transport patterns in 2014 and 2016 did not totally match the 2015 case, indicating future research ought to be carried out on a longer period and on multiple backgrounds. Based on obtaining at least one decade of historical meteorology data, one may conclude a certain transport pattern that can be taken advantage of to anticipate possible emission source regions and reduce corresponding pollution impacts.

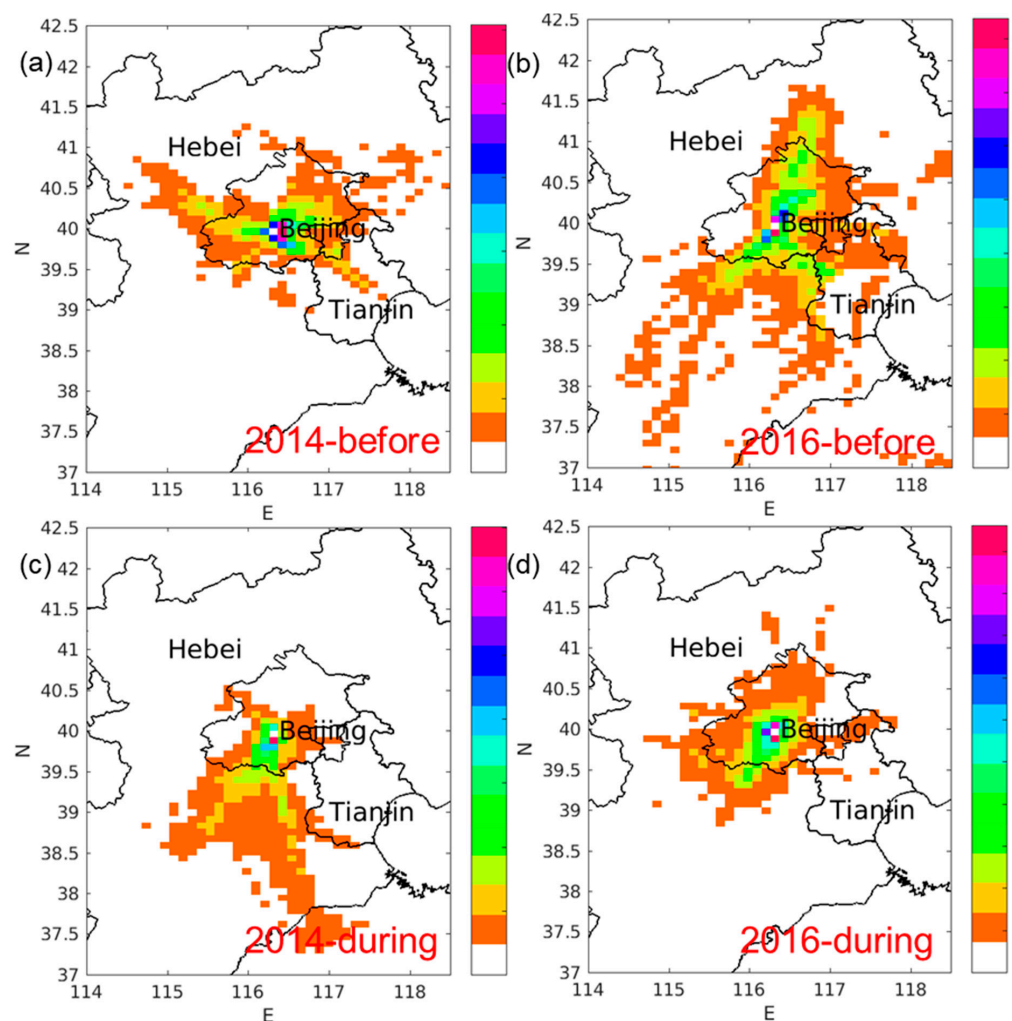
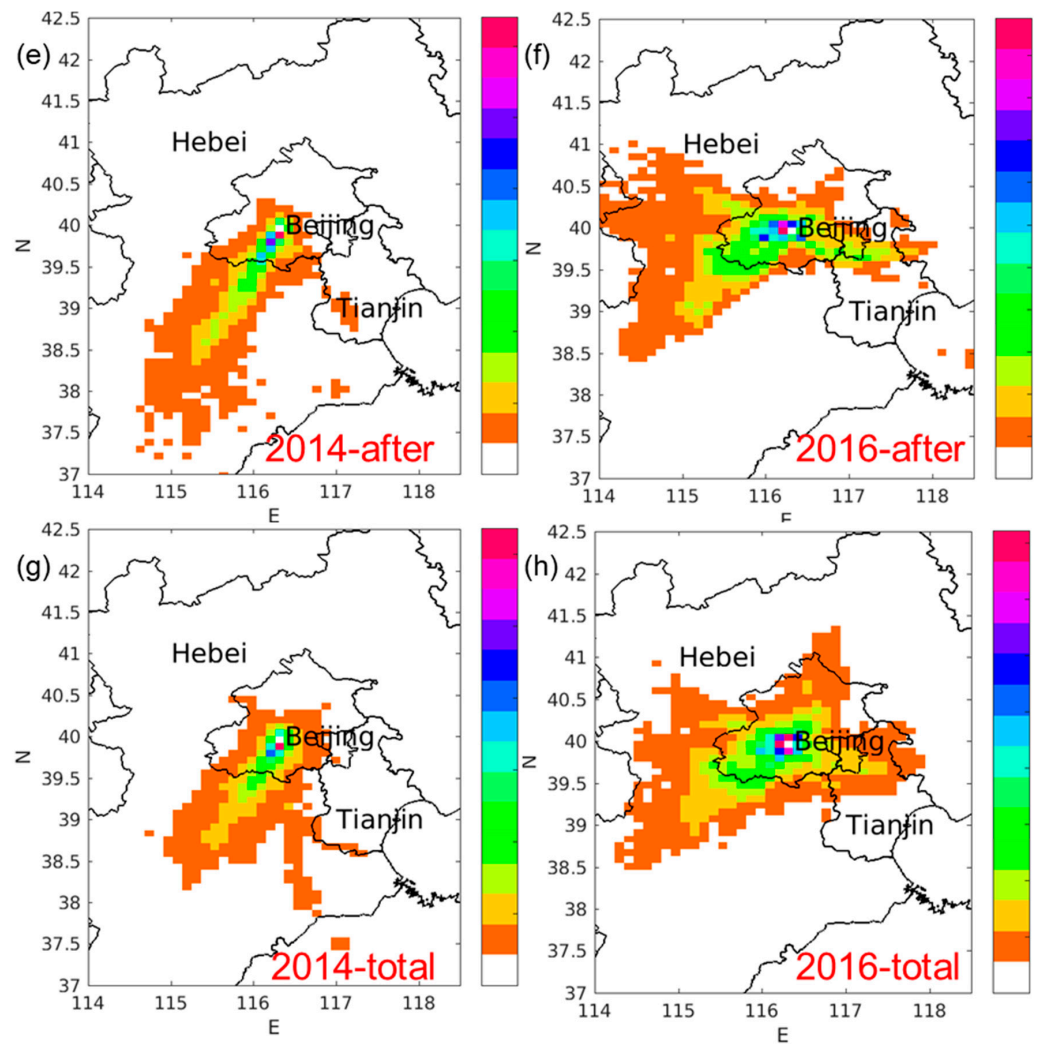
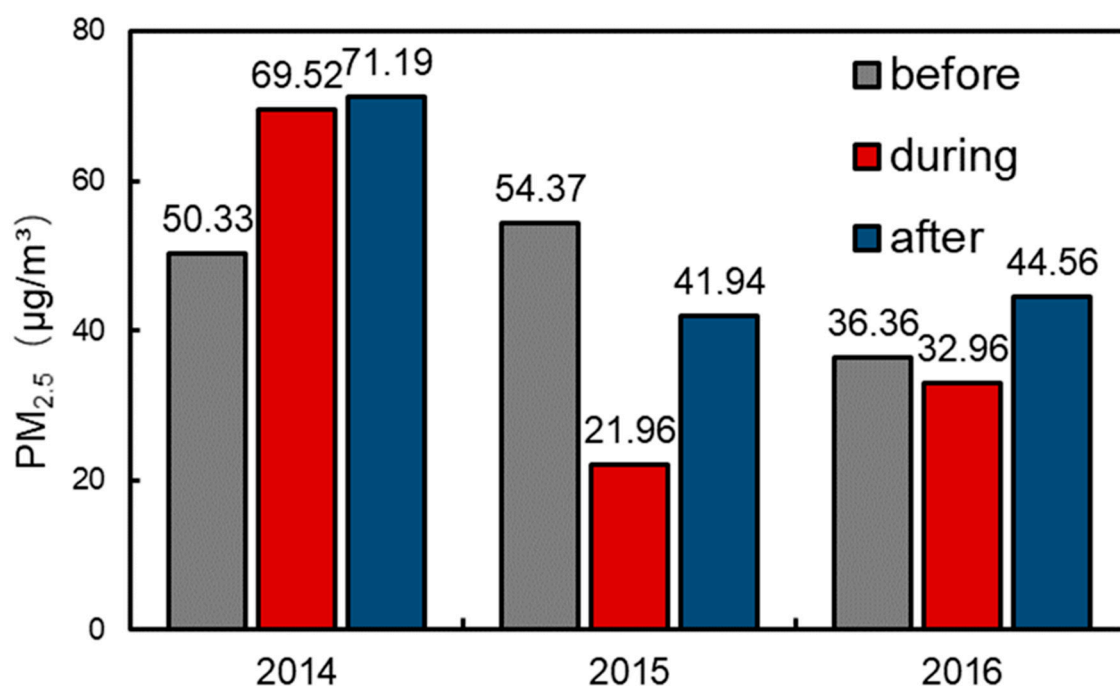


Figure 11. Cont.



**Figure 11.**  $PM_{2.5}$  CFAs comparison of 2014 and 2016 during the same sampling periods. Subplots (a,c,e,g) are the CFAs of the four periods in 2014. Subplots (b,d,f,h) are the CFAs of four periods in 2016. Other configurations and set-ups are the same in the MATLAB calculation scripts. From bottom to top side of the color bar, the cell contribution gets higher.

In fact, research on the potential source areas and transmission characteristics of the Beijing–Tianjin–Hebei region and its surrounding areas has been ongoing in recent years [37,45–51]. In this regard, more studies will analyze the transboundary transmission characteristics in this region from the perspective of models. Such studies also point out the possibility of transmission in the northeast, southwest, and even part of the northwest channels in the Beijing–Tianjin–Hebei region [45,46]. Among the three channels, Shijiazhuang, Zhangjiakou, and Chengde are all significant source cities. Other studies are seeking novel methods to demonstrate regional transmission, including determining the dominant transmission direction during heavy pollution periods or control periods, as well as quantitatively calculating the specific contribution rates of transmission channels to Beijing or other regions [46,48,49,52–54]. This study is based on a novel method of numerical simulation of atmospheric pollutant transport process in backward mode, and also located the main transmission channel and contribution of source area in BTH region, but further carried on the quantitative calculation of contribution to source area transmission. This calculation method and the concept of RTA and CFA overall are getting closer to the actual transmission process of atmospheric pollutants.



**Figure 12.** PM<sub>2.5</sub> average concentration in three periods in 2014, 2015, and 2016. The averaged time periods in 2014 and 2016 are both in consistent with 2015 as demonstrated in previous sessions.

#### 4. Conclusions

(1) PM<sub>2.5</sub>, gaseous compounds, and organic matter concentration showed evident reduction during the control period. Biomass burning and fossil fuel burning emissions were considered significantly reduced during the control period. They are highly correlated with industry, power, transportation, and partially agriculture and residential, which are mostly primary emissions. These sources were reduced significantly than other possible secondary sources.

(2) The long-range southeast path was the dominant direction during two separate non-control periods and contributed over 50% PM<sub>2.5</sub> to Beijing city, while the northeast path was the dominant transport path but with a significantly lower PM<sub>2.5</sub> contribution amount. The core potential emission source region from the southwest path area did not become the dominant source region to Beijing city during the control period. Instead, the proper relatively cleaner northeast area with Chengde city became the source region during the control period only contributed roughly one-third emission versus the southwest path.

(3) The meteorological conditions in the BTH region in fact determined the air quality in Beijing city during the control period and the air quality control policies implemented in some cities in central and southern Hebei province could be relaxed to some extent. Meteorological conditions prevent some major source regions from transporting massive pollutants. Some unnecessary economic damages should be avoided in future policy-making actions. A historical meteorological data and statistics analysis of the historical meteorological data should be done.

**Supplementary Materials:** The following are available online at <https://www.mdpi.com/article/10.3390/atmos12050636/s1>, **Table S1:** Correlation value (R) between PM<sub>2.5</sub>, SO<sub>2</sub>, CO, NO<sub>2</sub>, O<sub>3</sub>, OC and EC, **Table S2:** Total average concentration of aldehydes, alkanols, sterols in three time periods (ng/m<sup>3</sup>), **Table S3:** WRF simulation performance assessments. OM represents observation mean value. SM represents simulation mean value. R represents the Pearson correlation value. RMSE represents Root Mean Squared Error and MAE represents mean absolute error. **Table S4:** Contribution percentage (%) of long-range transport paths. SW represents the southeast path. NE represents the northeast path. Others contains all not significant transport contribution. Local

represents the transport within Beijing domain. The total column represents the whole sampling period. Only significant transport paths in CFA fields were calculated, **Figure S1**: CFA results of OC in four time periods. Subplots a, b, c and d are for before, during, after and the total observation periods, **Figure S2**: CFA results of EC in four time periods. Subplots a, b, c and d are for before, during, after and the total observation periods, **Figure S3**: The CFA results for three atmospheric pollutants, CO, NO<sub>2</sub> and SO<sub>2</sub>. Subplots a~d, e~h, and i~l are for CO, NO<sub>2</sub>, and SO<sub>2</sub>, respectively.

**Author Contributions:** Conceptualization, S.Y., Y.Z. (Yang Zhang), B.d.F., Y.Z. (Yuanxun Zhang); Data curation, S.Y., Y.Z. (Yang Zhang), J.S.; Formal analysis, S.Y.; Funding acquisition, Y.Z. (Yang Zhang), Y.Z. (Yuanxun Zhang); Investigation, Y.Z. (Yang Zhang), J.J.S.; Methodology, S.Y., J.S., Z.L., J.J.S.; Project administration, Y.Z. (Yang Zhang); Resources, Z.L., B.d.F., J.J.S., Y.Z. (Yuanxun Zhang), Software, S.Y., B.d.F.; Supervision, Y.Z. (Yang Zhang), Y.Z. (Yuanxun Zhang); Visualization, S.Y., B.d.F.; Writing—original draft, S.Y., Writing—review & editing, S.Y., Y.Z. (Yang Zhang), Y.Z. (Yuanxun Zhang). All authors have read and agreed to the published version of the manuscript.

**Funding:** This research was funded by Fundamental Research Funds for the Central Universities (No. E0E48927X2) and National Key Research and Development Program of China (No. 2016YFC0503600) and the Major Science and Technology Projects of Qinghai Province in 2018 (2018-SF-A4). The APC was funded by National Key R&D Program of China (2016YFC0503605).

**Institutional Review Board Statement:** Not applicable.

**Informed Consent Statement:** Not applicable.

**Data Availability Statement:** The data presented in this study are available on request from the corresponding author.

**Conflicts of Interest:** The authors declare no conflict of interest.

## References

- Li, X.; Zhang, C.; Li, W.; Anyah, R.O.; Tian, J. Exploring the trend, prediction and driving forces of aerosols using satellite and ground data, and implications for climate change mitigation. *J. Clean. Prod.* **2019**, *223*, 14. [\[CrossRef\]](#)
- Chuang, M.-T.; Chel Gee Ooi, M.; Lin, N.-H.; Fu, J.S.; Lee, C.-T.; Wang, S.-H.; Yen, M.-C.; Kong, S.S.-K.; Huang, W.-S. Study on the impact of three Asian industrial regions on PM<sub>2.5</sub> in Taiwan and the process analysis during transport. *Atmos. Chem. Phys.* **2020**, *20*, 21. [\[CrossRef\]](#)
- Li, P.; Xiao, Z.; Tang, M.; Xu, H.; Li, L.; Chen, K.; Deng, X. Particulate Pollution Characteristics of Typical Sand Dust Wearthe in Tianjin. *J. Ecol. Rural Environ.* **2020**, *36*, 8. [\[CrossRef\]](#)
- Li, X.; Zhang, C.; Li, W.; Liu, K. Evaluating the Use of DMSP/OLS Nighttime Light Imagery in Predicting PM<sub>2.5</sub> Concentrations in the Northeastern United States. *Remote Sens.* **2017**, *9*, 16. [\[CrossRef\]](#)
- Cheng, N.L.; Zhang, D.W.; Li, Y.T.; Chen, T.; Sun, F.; Li, L.J.; Cheng, B.F. Characteristics of NO<sub>x</sub> concentrations during IAAF World Championships in Athletics and 9.3 military parade periods in 2015 in Beijing. *J. Univ. Chin. Acad. Sci.* **2016**, *33*, 834–843. [\[CrossRef\]](#)
- Zhao, H.; Zheng, Y.F.; Xu, J.X.; Wang, Z.S.; Yuan, Y.; Huang, J.Q.; Chu, Z.F. Evaluation of the improvement of the air quality during the parade in Beijing. *China Environ. Sci.* **2016**, *36*, 2881–2889.
- Jia, J.; Guo, X.R.; Cheng, S.Y. Numerical study on the characteristics of PM<sub>2.5</sub> in Beijing and the assessment of pollution control measures during APEC. *China Environ. Sci.* **2016**, *36*, 2337–2346.
- Wu, Y.F.; Guan, Y.C.; Dong, H.Y. Variations of Water Soluble Ions in PM<sub>2.5</sub> during the Asia-Pacific Economic Cooperation Summit in Tianjin and Surrounding Cities. *Environ. Sustain. Dev.* **2016**, *6*, 213–217.
- Zhou, J.B.; Li, Z.G.; Lu, N.; Xu, M.; Yang, P.; Gao, K.N.; Wang, J.G.; Jin, W. Online Sources about Atmospheric Fine Particles During the 70th Anniversary of Victory Parade in Shijiazhuang. *Environ. Sci.* **2016**, *37*. [\[CrossRef\]](#)
- Zhang, J.; Song, X.H. Environmental and Meteorological Conditions and Effect of Emergency Emission Reduction in South Hebei. *Chin. Agric. Sci. Bull.* **2016**, *32*, 153–158. [\[CrossRef\]](#)
- Lv, Z.; Cheng, S.Y.; Yang, X.W. Characterization and sources of Carbon components in PM<sub>2.5</sub> from Tang Shan city before and after the Military Parade. In Proceedings of the Annual Conference of the Chinese Society for Environmental Sciences, Haikou, Hainan, China, 6–8 September 2016; pp. 2621–2627.
- Tao, J.; Gao, J.; Zhang, L.M.; Wang, H.; Qiu, X.H.; Zhang, Z.S.; Wu, Y.F.; Chai, F.H.; Wang, S.L. Chemical and optical characteristics of atmospheric aerosols in Beijing during the Asia-Pacific Economic Cooperation China 2014. *Atmos. Environ.* **2016**, *144*, 8–16. [\[CrossRef\]](#)
- Yang, H.; Wang, S.X.; Wang, J.D.; Jiang, J.K.; Zhang, T.S.; Song, Y.; Kang, L.; Zhou, W.; Cai, R.L.; Wu, D.; et al. Investigating the impact of regional transport on PM<sub>2.5</sub> formation using vertical observation during APEC 2014 Summit in Beijing. *Atmos. Chem. Phys.* **2016**, *16*, 15451–15460. [\[CrossRef\]](#)

14. Liu, H.L.; He, J.; Guo, J.P.; Miao, Y.C.; Yin, J.F.; Wang, Y.; Xu, H.; Liu, H.; Yan, Y.; Li, Y.; et al. The blue skies in Beijing during APEC 2014: A quantitative assessment of emission control efficiency and meteorological influence. *Atmos. Environ.* **2017**, *167*, 235–244. [[CrossRef](#)]
15. Xu, W.; Song, W.; Zhang, Y.Y.; Liu, X.J.; Zhang, L.; Zhao, Y.H.; Liu, D.Y.; Tang, A.H.; Yang, D.W.; Wang, D.D.; et al. Air quality improvement in a megacity: Implications from 2015 Beijing Parade Blue pollution control actions. *Atmos. Chem. Phys.* **2017**, *17*, 31–46. [[CrossRef](#)]
16. Cass, G.R. Organic molecular tracers for particulate air pollution sources. *Trends Anal. Chem.* **1998**, *17*, 356–366. [[CrossRef](#)]
17. Schauer, J.J.; Kleeman, M.J.; Cass, G.R.; Simoneit, B.R.T. Measurement of emissions from air pollution sources. 3. C1-C29 organic compounds from fireplace combustion of wood. *Environ. Sci. Technol.* **2001**, *35*, 1716–1728. [[CrossRef](#)]
18. Zhang, Y.X.; Shao, M.; Zhang, Y.H.; Zeng, L.M.; He, L.Y.; Zhu, B.; Wei, Y.J.; Zhu, X.L. Source profiles of particulate organic matters emitted from cereal straw burnings. *J. Environ. Sci.* **2007**, *19*, 167–175. [[CrossRef](#)]
19. Zhang, Y.X.; Schauer, J.J.; Zhang, Y.H.; Zeng, L.M.; Wei, Y.J.; Liu, Y.; Shao, M. Characteristics of particulate carbon emissions from real-world Chinese coal combustion. *Environ. Sci. Technol.* **2008**, *42*, 5068–5073. [[CrossRef](#)]
20. Stone, E.A.; Snyder, D.C.; Sheesley, R.J.; Sullivan, A.P.; Weber, R.J.; Schauer, J.J. Source apportionment of fine organic aerosol in Mexico City during the MILAGRO experiment 2006. *Atmos. Chem. Phys.* **2008**, *8*, 1249–1259. [[CrossRef](#)]
21. Sheesley, R.J.; Schauer, J.J.; Chowdhury, Z.; Cass, G.R.; Simoneit, B.R.T. Characterization of organic aerosols emitted from the combustion of biomass indigenous to South Asia. *J. Geophys. Res. Atmos.* **2003**, *108*. [[CrossRef](#)]
22. Herner, J.D.; Green, P.G.; Kleeman, M.J. Measuring the Trace Elemental Composition of Size-Resolved Airborne Particles. *Environ. Sci. Technol.* **2006**, *40*, 1925–1933. [[CrossRef](#)] [[PubMed](#)]
23. Schauer, J.J.; Mader, B.T.; Deminter, J.T.; Heidemann, G.; Bae, M.S.; Seinfeld, J.H.; Flagan, R.C.; Cary, R.A.; Smith, D.; Huebert, B.J.; et al. ACE-Asia Intercomparison of a Thermal-Optical Method for the Determination of Particle-Phase Organic and Elemental Carbon. *Environ. Sci. Technol.* **2003**, *37*, 993–1001. [[CrossRef](#)] [[PubMed](#)]
24. Huan, N.; Zhou, N.; Zeng, L.M.; Dong, H.B.; Shao, M.; Yu, Z.Y.; Cui, L.; Luo, Z.M.; Mao, J.T. Measurement and Discussion of Carbonaceous PM<sub>2.5</sub> during Winter in Beijing. *Acta Sci. Nat. Univ. Pekin.* **2006**, *42*, 265–270. [[CrossRef](#)]
25. Bae, M.S.; Hong, C.S.; Kim, Y.J.; Han, J.S.; Moon, K.J.; Kondo, Y.; Komazaki, Y.; Miyazaki, Y. Intercomparison of two different thermal-optical elemental carbons and optical black carbon during ABC-EAREX2005. *Atmos. Environ.* **2007**, *41*, 2791–2803. [[CrossRef](#)]
26. Zhang, Y.X. *Study on Speciation of Particulate Organic Matter from Combustion Sources*; Beking University: Beijing, China, 2006.
27. Castro, L.M.; Pio, C.A.; Harrison, R.M.; Smith, D.J.T. Carbonaceous aerosol in urban and rural European atmospheres: Estimation of secondary organic carbon concentrations. *Atmos. Environ.* **1999**, *33*, 2771–2781. [[CrossRef](#)]
28. Brioude, J.; Arnold, D.; Stohl, A.; Cassiani, M.; Morton, D.; Seibert, P.; Angevine, W.; Evan, S.; Dingwell, A.; Fast, J.D.; et al. The Lagrangian particle dispersion model FLEXPART-WRF version 3.1. *Geosci. Model Dev.* **2013**, *6*, 1889–1904. [[CrossRef](#)]
29. Wang, W.; Bruyère, C.; Duda, M.; Dudhia, J.; Gill, D.; Kavulich, M.; Keene, K.; Lin, H.-C.; Michalakes, J.; Rizvi, S.; et al. *ARW Version 3 Modeling System User's Guide*; NCAR: Boulder, CO, USA, 2015.
30. De Foy, B.; Krotkov, N.A.; Bei, N.; Herndon, S.C.; Huey, L.G.; Mart'inez, A.-P.; Ruiz-Su'arez, L.G.; Wood, E.C.; Zavala, M.; Molina, L.T. Hit from both sides: Tracking industrial and volcanic plumes in Mexico City with surface measurements and OMI SO<sub>2</sub> retrievals during the MILAGRO field campaign. *Atmos. Chem. Phys.* **2009**, *9*, 9599–9617. [[CrossRef](#)]
31. Heo, J.b.; de Foy, B.; Olson, M.R.; Pakbin, P.; Sioutas, C.; Schauer, J.J. Impact of regional transport on the anthropogenic and biogenic secondary organic aerosols in the Los Angeles Basin. *Atmos. Environ.* **2015**, *103*, 171–179. [[CrossRef](#)]
32. De Foy, B.; Caetano, E.; Magana, V.; Zit'acuaro, A.; C'ardenas, B.; Retama, A.; Ramos, R.; Molina, L.T.; Molina, M.J. Mexico City basin wind circulation during the MCMA-2003 field campaign. *Atmos. Chem. Phys.* **2005**, *5*, 2267–2288. [[CrossRef](#)]
33. Ashbaugh, L.L.; Malm, W.C.; Sadeh, W.Z. A residence time probability analysis of sulfur concentrations at grand canyon national park. *Atmos. Environ.* **1985**, *19*, 1263–1270. [[CrossRef](#)]
34. De Foy, B.; Lei, W.; Zavala, M.; Volkamer, R.; Samuelsson, J.; Mellqvist, J.; Galle, B.; Mart'inez, A.-P.; Grutter, M.; Retama, A.; et al. Modelling constraints on the emission inventory and on vertical dispersion for CO and SO<sub>2</sub> in the Mexico City Metropolitan Area using Solar FTIR and zenith sky UV spectroscopy. *Atmos. Chem. Phys.* **2007**, *7*, 781–801. [[CrossRef](#)]
35. Stohl, A.; Hittenberger, M.; Wotawa, G. Validation of the lagrangian particle dispersion model flexpart again large-scarle tracer experiment data. *Atmos. Environ.* **1998**, *32*, 4245–4264. [[CrossRef](#)]
36. Wang, Y.Q.; Zhang, X.Y.; Draxler, R.R. TrajStat: GIS-based software that uses various trajectory statistical analysis methods to identify potential sources from long-term air pollution measurement data. *Environ. Model. Softw.* **2009**, *24*, 938–939. [[CrossRef](#)]
37. Zhou, L.; Wu, J.J.; Jia, R.J.; Liang, N.; Zhang, F.Y.; Ni, Y.; Liu, M. Investigation of Temporal-Spatial Characteristics and Underlying Risk Factors of PM<sub>2.5</sub> Pollution in Beijing-Tianjin-Hebei Area. *Res. Environ. Sci.* **2016**, *29*, 483–493.
38. Li, B.; Chen, C.H.; Yu, J.X. Designing photochemical smog pollution regional total control schemes by using EKMA diagram. *Plateau Meteorol.* **1998**, *2*, 111–119. [[CrossRef](#)]
39. EPA. *Guideline For Use of City-specific EKMA in Preparing Ozone SIPs*; U.S. Environmental Protection Agency: Washington, DC, USA, 1981.
40. Fang, D.Q.; Wei, Y.J.; Huang, W.; Cai, T.Q.; Zhang, Y.; Liu, Q.Y.; Zhang, Y.X. Characterization and Source Apportionment of Organic Carbon during a Heavy Haze Episode in Beijing in October 2014. *Res. Environ. Sci.* **2016**, *29*, 12–19. [[CrossRef](#)]

41. He, L.Y.; Hu, M.; Huang, X.F.; Zhang, Y.H. Determination of organic molecular tracers in PM<sub>2.5</sub> in the atmosphere of Beijing. *Acta Sci. Circumstantiae* **2005**, *25*, 23–29. [[CrossRef](#)]
42. Qu, Q.; Zhang, Z.S.; Liu, S.X.; Zhu, L.H. Characterization and Sources of Water-soluble Organic Carbon in PM<sub>2.5</sub> at Urban Guangzhou. *Environ. Sci. Technol.* **2015**, *38*. [[CrossRef](#)]
43. Li, J.; Xie, S.D.; Zeng, L.M.; Li, L.Y.; Li, Y.Q.; Wu, R.R. Characterization of ambient volatile organic compounds and their sources in Beijing, before, during, and after Asia-Pacific Economic Cooperation China 2014. *Atmos. Chem. Phys.* **2015**, *15*, 7945–7959. [[CrossRef](#)]
44. *Urban System Planning of Hebei Province (2016–2030)*; Hebei Provincial Department of Housing and Urban-Rural Development Hebei: Shijiazhuang, China, 2017.
45. Yao, S.; Zhang, H.-Y.; Wang, X.-Q.; Yang, S.-S. Air Pollution Characteristics and Quantitative Evaluation of Multi-scale Transport in the Beijing-Tianjin-Hebei Region in January 2016. *Environ. Sci.* **2021**, *42*, 12. [[CrossRef](#)]
46. Zhang, H.; Xing, Y.; Cheng, S.; Wang, X.; Guan, P. Characterization of multiple atmospheric pollutants during haze and non-haze episodes in Beijing, China: Concentration, chemical components and transport flux variations. *Atmos. Environ.* **2021**, *246*, 13. [[CrossRef](#)]
47. Zhao, X.; Shen, N.-C.; Li, L.-J.; Wu, G.-F.; Tao, J.; Zhao, W.-J. Analysis of Changes and Factors Influencing Air Pollutants in the Beijing-Tianjin-Hebei Region During the COVID-19 Pandemic. *Environ. Sci.* **2021**, *42*, 10. [[CrossRef](#)]
48. Lv, L.; Chen, Y.; Han, Y.; Cui, M.; Wei, P.; Zheng, M.; Hu, J. High-time-resolution PM<sub>2.5</sub> source apportionment based on multi-model with organic tracers in Beijing during haze episodes. *Sci. Total Environ.* **2021**, *772*, 11. [[CrossRef](#)]
49. Wu, J.; Bei, N.; Wang, Y.; Li, X.; Liu, S.; Liu, L.; Wang, R.; Yu, J.; Le, T.; Zuo, M.; et al. Insights into particulate matter pollution in the North China Plain during wintertime: Local contribution or regional transport? *Atmos. Chem. Phys.* **2021**, *21*, 2229–2249. [[CrossRef](#)]
50. Zhang, Q.; Shen, Z.; Zhang, T.; Kong, S.; Lei, Y.; Wang, Q.; Tao, J.; Zhang, R.; Wei, P.; Wei, C.; et al. Spatial distribution and sources of winter black carbon and brown carbon in six Chinese megacities. *Sci. Total Environ.* **2021**, *762*, 12. [[CrossRef](#)] [[PubMed](#)]
51. Zhao, S.; Tian, H.; Luo, L.; Liu, H.; Wu, B.; Liu, S.; Bai, X.; Liu, W.; Liu, X.; Wu, Y.; et al. Temporal variation characteristics and source apportionment of metal elements in PM<sub>2.5</sub> in urban Beijing during 2018–2019. *Environ. Pollut.* **2021**, *268*, 13. [[CrossRef](#)]
52. Liu, Y.; Tang, G.; Wang, M.; Liu, B.; Hu, B.; Chen, Q.; Wang, Y. Impact of residual layer transport on air pollution in Beijing, China. *Environ. Pollut.* **2021**, *271*, 8. [[CrossRef](#)]
53. Guan, P.; Wang, X.; Cheng, S.; Zhang, H. Temporal and spatial characteristics of PM<sub>2.5</sub> transport fluxes of typical inland and coastal cities in China. *J. Environ. Sci.* **2021**, *103*, 17. [[CrossRef](#)] [[PubMed](#)]
54. Ansari, T.U.; Wild, O.; Ryan, E.; Chen, Y.; Li, J.; Wang, Z. Temporally resolved sectoral and regional contributions to air pollution in Beijing: Informing short-term emission controls. *Atmos. Chem. Phys.* **2021**, *21*, 15. [[CrossRef](#)]